

Modeling atmospheric sulfur over the Northern Hemisphere during the Aerosol Characterization Experiment 2 experimental period

Carmen M. Benkovitz,¹ Stephen E. Schwartz,¹ Michael P. Jensen,² Mark A. Miller,¹ R. C. Easter,³ and Timothy S. Bates⁴

Received 21 April 2004; revised 1 July 2004; accepted 15 August 2004; published 25 November 2004.

[1] A high-resolution ($1^\circ \times 1^\circ$, 27 vertical levels) Eulerian chemical transport and transformation model for sulfate, SO_2 , and related species driven by analyzed forecast meteorological data has been run for the Northern Hemisphere for June–July 1997 and extensively evaluated with observational data, mainly from air quality and precipitation chemistry networks. For ~ 5000 evaluations, 50% of the modeled sulfate 24-hour mixing ratios were within a factor of 1.85 of the observations; 50% of ~ 328 concurrent subgrid observations were within a factor of 1.33. Much greater subgrid variation for 24-hour SO_2 mixing ratios (50% of ~ 3552 observations were within a factor of 2.32) reflects high variability of this primary species; for ~ 12600 evaluations, 50% of modeled mixing ratios were within a factor of 2.54 of the observations. These results indicate that a substantial fraction of the modeled and observed differences is due to subgrid variation and/or measurement error. Sulfate mixing ratios are identified by source type (biogenic, volcanic, and anthropogenic) and production mechanism (primary and by gas-phase and aqueous-phase oxidation). Examination of key diagnostics showed substantial variation for the different types of sulfur, e.g., SO_2 aqueous-phase oxidation rates of 29–102% d^{-1} and sulfate residence times of 4–9 days. Volcanic emissions contributed 10% of the sulfate burden and 6% of emissions, because the elevated release allows large fractional conversion of SO_2 and long residence time. Biogenic SO_2 was generally at lower concentrations than H_2O_2 , resulting in efficient aqueous-phase oxidation; this source type contributed 13% of emissions but only 5% of sulfate burden. Anthropogenic sources were the dominant contributors to sulfur emissions (80%) and sulfate burden (84%).

INDEX TERMS: 0305 Atmospheric Composition and Structure: Aerosols and particles (0345, 4801); 0322 Atmospheric Composition and Structure: Constituent sources and sinks; 0365 Atmospheric Composition and Structure: Troposphere—composition and chemistry; 0368 Atmospheric Composition and Structure: Troposphere—constituent transport and chemistry; 0399 Atmospheric Composition and Structure: General or miscellaneous; **KEYWORDS:** sulfate, modelling, CTM

Citation: Benkovitz, C. M., S. E. Schwartz, M. P. Jensen, M. A. Miller, R. C. Easter, and T. S. Bates (2004), Modeling atmospheric sulfur over the Northern Hemisphere during the Aerosol Characterization Experiment 2 experimental period, *J. Geophys. Res.*, *109*, D22207, doi:10.1029/2004JD004939.

1. Introduction

[2] Atmospheric aerosols are recognized to have provided a substantial secular forcing of climate change over the industrial period, but of highly uncertain magnitude [Ramaswamy *et al.*, 2001]; therefore it is essential that aerosol radiative forcing be well quantified and accurately represented in climate models to provide a sound basis for formulating policy regarding the reduction of anthropogenic influences on climate. Representations of aerosol processes

in chemical transport models (CTMs) are necessary to develop and test such representations for use in climate models [National Research Council Panel on Aerosol Radiative Forcing and Climate, 1996]. Intercontinental transport of aerosols has been demonstrated by in situ measurements [Jaffe *et al.*, 2003; Prospero, 1999; Talbot *et al.*, 1986; Wotawa and Trainer, 2000] and by satellite observations that have followed the plumes of smoke from forest fires over thousands of kilometers [Heald *et al.*, 2003; Prasad *et al.*, 2002; Wooster and Strub, 2002]; the causes and effects of events such as these can be better determined if CTMs allocate aerosol loadings by source regions, source types, and formation processes. Because of the highly nonuniform distribution of the sources of accumulation mode aerosol particles, their spatially and temporally intermittent removal, and their short atmospheric residence times, about a week [e.g., Cambray *et al.*, 1987; Chamberlain, 1991], representation of the processes governing the geo-

¹Brookhaven National Laboratory, Upton, New York, USA.

²Department of Applied Physics and Applied Mathematics, Columbia University, New York, USA.

³Pacific Northwest National Laboratory, Richland, Washington, USA.

⁴Pacific Marine Environmental Laboratory, Seattle, Washington, USA.

graphical distribution of these particles in CTMs and evaluation of model performance require high space (≤ 400 km) and time (≤ 24 hours) resolution [Benkovitz *et al.*, 1994].

[3] A major component of aerosols in industrialized regions of the world is sulfate resulting from the oxidation of anthropogenic sulfur dioxide (SO_2) [U.S. Environmental Protection Agency, 2001]. On regional and local scales this sulfate has been linked to adverse health effects [Vedal, 1997], visibility impairment [U.S. Environmental Protection Agency, 2001], ecological damage [Kuylenstierna *et al.*, 2001], and acid rain [Cowling, 1982]. Sulfate has become a valuable test bed for CTMs representing aerosols for several reasons: its importance as an anthropogenic species, fairly well developed emissions inventories, emissions with rather low temporal variability, and well understood atmospheric chemistry albeit with complexities arising from production by both gas-phase and aqueous-phase reactions.

[4] Several models that include representations of the sulfur cycle have been developed, for example [Barth *et al.*, 2000; Chin *et al.*, 2000a, 2000b; Koch *et al.*, 1999; Langner and Rodhe, 1991; Rasch *et al.*, 2000a; Roelofs *et al.*, 1998], and intercomparisons of global-scale model results have been conducted [Barrie *et al.*, 2001; Lohmann *et al.*, 2001; Penner *et al.*, 2001; Rasch *et al.*, 2000b; Roelofs *et al.*, 2001]. A majority of the models are general circulation models (GCMs) with sulfur chemistry added or are driven by meteorological data from GCMs; such models have the advantage of being able to generate statistics on monthly and annual mean concentrations. However, because sulfate concentrations are highly variable because of meteorological variability, the results from such models can be compared to observations only in rather long temporal averages and do not permit comparison with specific episodes or individual days. Thus comparison studies with such models typically report results in terms of annual or seasonal averages, with limited quantitative statistics as a consequence of the small number of samples.

[5] Two recent intercomparison studies examined model results and attempted to account for the differences found. Comparison of the results of nine models [Barrie *et al.*, 2001] found that differences in representations of processes in the models resulted in rather large differences in the relative importance of different processes in the sulfur cycle; for example, estimates of the fraction of total sulfur removed by dry deposition in the several models ranged from 36 to 54%, residence times ranged from 3.6 to 7.5 days for sulfate, from 1.3 to 3.1 days for SO_2 , and from 1 to 3.9 days for DMS. The dominant cause of model-to-model differences in regional sulfur budgets within emissions source regions was found to be the representations of in-cloud processes: aqueous-phase oxidation, wet deposition, and vertical transport; outside the source regions the efficiency of horizontal transport is also of importance. In spite of such differences most models predicted surface seasonal mean sulfate MRs within 20%; this suggests the need for finer spatial and temporal resolution in the comparison of model results with observations, and more detailed examination of how the differences in process representations interact, perhaps via compensating errors, to produce similar results. The results of eleven models were examined at a series of remote surface stations by Penner *et al.* [2001]; the enve-

lope of the modeled annual average sulfate concentrations was between 0.1 and $3 \mu\text{g}^{-3}$, and excluding model results that were considered outliers on the basis of their comparisons with observations, the spread of the estimated sulfate aerosol burden was a factor of 2.2. There is thus a great need to understand these differences between models; both studies recommended more detailed measurements, especially in remote areas and in the vertical, against which to test model parameterizations of aerosol processes as well as model results.

[6] The work reported here is a study conducted using the Global Chemistry Model Driven By Observation-Derived Meteorology (GChM-O), a Eulerian CTM that represents the sulfur cycle and calculates distributions of sulfate, SO_2 , dimethyl sulfide (DMS), and methanesulfonic acid (MSA) with high spatial and temporal resolution, for specific times and locations, by source region, source type, and sulfate formation process. A previous study reported results from calculations using an earlier version of this model and extensive comparisons with observations in simulations of four seasonal six-week periods in 1986–1987 [Benkovitz *et al.*, 1994; Benkovitz and Schwartz, 1997]. Because the model was driven by analyzed forecast meteorological data it was possible to obtain extensive evaluation of model results and observed mixing ratios (MRs) for short periods of time (typically 24 hours as governed by measurement protocols) and at numerous locations. Benkovitz and Schwartz [1997] reported approximately 8000 model observation evaluations for sulfate and approximately 20,000 evaluations for SO_2 ; a large fraction of the departure between modeled and observed MRs was attributed to subgrid variability and/or nonrepresentative sampling of model grid cells at the stations used for the evaluations.

[7] The present version of the model includes refined parameterizations of chemical mechanisms, aerosol uptake by clouds, and wet removal. In the previous subhemispheric model (140°W to 60°E longitude) much of the sulfate aerosol was exported from the modeling domain; therefore the domain of the current model has been expanded to include the Northern Hemisphere from the equator to 81°N . This expanded domain incorporates all industrialized areas of the hemisphere and allows examination of the influence of the several major source regions. This version of the model has been used to simulate the period of the Aerosol Characterization Experiment 2 (ACE-2), which took place in June–July 1997 over the eastern North Atlantic [Raes *et al.*, 2000].

[8] Measurements conducted as part of ACE-2 obtained high space and time resolution observations of the concentrations of aerosols and precursor species; measurements taken at Tenerife, Canary Islands, and at Sagres, Portugal, permitted a case study of results of the model simulation in this region [Benkovitz *et al.*, 2003]. Detailed evaluations of the simulation results demonstrated that the model was capable of representing sulfate MRs at Tenerife (minimal influence from proximate sources) within the intermeasurement and subgrid variations. At Sagres (influenced by proximate sources) the spread between model and observations was larger; this was attributed to the nonrepresentativeness of a single measurement at a location where considerable subgrid variation can be expected. Although Tenerife is geographically much closer to Europe than to

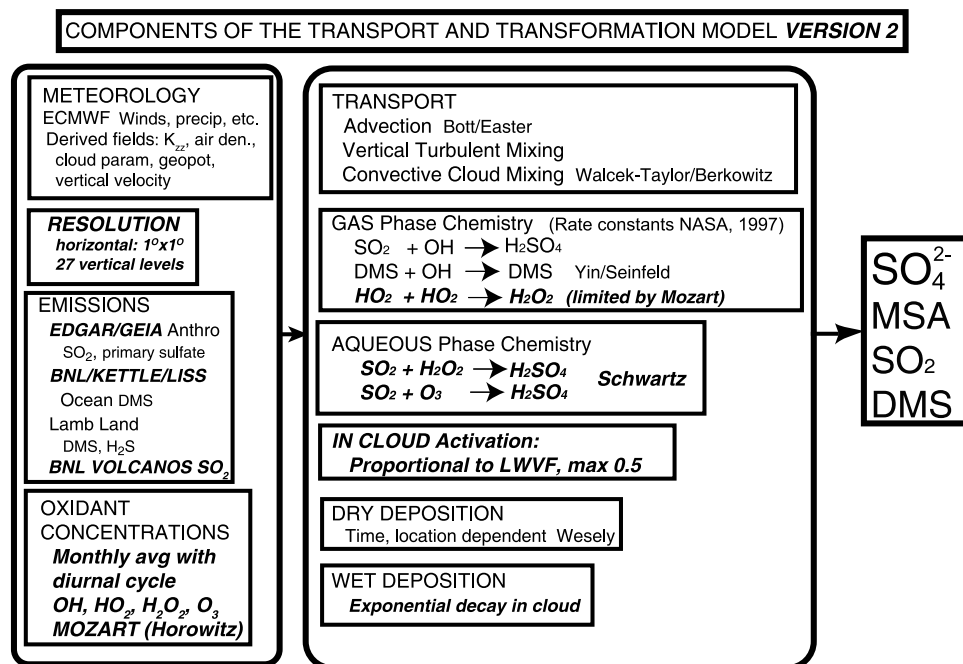


Figure 1. Schematic of the processes included in the Global Chemistry Model Driven by Observation-Derived Meteorology (GChM-O). See Table 2 for the description of the meteorology-derived fields. Bold oblique characters indicate changes in Version 2. Here, BNL/Kettle/Liss, Brookhaven National Laboratory, Kettle *et al.* [1999], and Liss and Merlivat [1986]; Lamb, B. Lamb (Bates *et al.* [1992]); Horowitz, Horowitz *et al.* [2003]; Bott/Easter, Bott [1989], Easter [1993], and Easter and Luecken [1988]; Walcek-Taylor/Berkowitz, Walcek and Taylor [1986]; NASA 1997 refers to Demore *et al.* [1997]; Yin/Seinfeld, Yin *et al.* [1990a, 1990b]; Schwartz, Schwartz [1988]; and Wesely, Sheih *et al.* [1986], Wesely [1989], and Benkovitz *et al.* [1994].

North America, the contributions from European, North American, and biogenic sources to the sulfate burden in this time period were comparable at this location, with North American sources dominating (up to $\sim 85\%$) under conditions of a strong Azores high.

[9] The work described here extends the evaluation of model results using observations from routine air quality monitoring stations in North America, Europe, and Taiwan, and stations in the Canary Islands and Korea. Measures of rates and extent of important processes (yields, conversion, removal rates, etc.) calculated from model results are reported, permitting comparison of these quantities as represented in other models.

2. Description of the Model

[10] The model used in this study is a three-dimensional Eulerian transport and transformation model for sulfate,

MSA, and precursor species. Species abundance is reported as mixing ratio (MR, mol per mol air; $1 \text{ nmol mol}^{-1} = 1 \text{ ppb}$), as this quantity is invariant to expansion and compression because of fluctuations in pressure and temperature. The model represents emissions of SO_2 and DMS, transport, convective mixing, conversion of SO_2 to sulfate by H_2O_2 and O_3 in the aqueous phase and by OH in the gas phase, gas-phase conversion of DMS to SO_2 and MSA by OH, wet removal, and dry deposition. The model domain includes the entire Northern Hemisphere from the equator to 81°N , and because this domain is not global, it is necessary to account for material advected into the model domain by assigning representative background concentrations; this external material is carried as separate variables. The model is initialized with the mixing ratio of all species set to zero. The processes represented in GChM-O Version 2 are outlined in Figure 1, the chemical species represented in the model are defined in Table 1 and the model input data and

Table 1. Sulfur Species Defined in the Model

Source	SO_2		Sulfate			DMS Primary	MSA Gas-Phase Oxidation
	Primary	Gas-Phase Oxidation	Primary	Gas-Phase Oxidation	Aqueous-Phase Oxidation		
North America anthropogenic 140°W to 30°W	X		X	X	X		
Europe anthropogenic 30°W to 60°E	X		X	X	X		
Asia anthropogenic 60°E to 140°W	X		X	X	X		
Volcanic	X			X	X		
Biogenic		X		X	X	X	
External	X		X	X	X		

Table 2. Input Data Used in the Model and Their Provenance

Quantity	Provenance
<i>Meteorology: 2-D Fields</i>	
Cloud base	based on ECMWF data
Cloud top	based on ECMWF data
Low, medium, and high cloud cover	ECMWF
Stratiform cloud cover	ECMWF
Total cloud cover	ECMWF
Convective precipitation	ECMWF
Stratiform precipitation	ECMWF
Surface pressure	ECMWF
Surface temperature	ECMWF
Solar zenith angle	calculated on the basis of location and time
SO ₂ , sulfate, and H ₂ O ₂ dry deposition velocities	Wesely ^a
<i>Meteorology: 3-D Fields</i>	
Geopotential	based on ECMWF algorithm
Cloud liquid water content	ECMWF
Convective cloud mixing fraction	based on ECMWF data
Air density	based on ECMWF data
Specific humidity	ECMWF
<i>u</i> and <i>v</i> components of wind	ECMWF
Vertical velocity <i>w</i>	based on ECMWF algorithm
Temperature	ECMWF
Pressure	based on ECMWF algorithm
Vertical diffusivity coefficient <i>K_{zz}</i>	calculated, section 2.1.1
<i>Oxidant Concentrations: 3-D Fields</i>	
OH, H ₂ O ₂ , O ₃ , and HO ₂ mixing ratios	MOZART ^b
<i>Emissions: 2-D Fields</i>	
Oceanic DMS	calculated from surface ocean DMS ^c
Land DMS	B. Lamb ^d
<i>Emissions: 3-D Fields</i>	
Anthropogenic SO ₂ and primary sulfate	EDGAR V3.2 ^e
Volcanic SO ₂	calculated, section 2.4.3.

^aCalculated according to M. Wesely (as provided by Sheih *et al.* [1986] and Wesely [1989]) and Benkovitz *et al.* [1994].

^bJune–July averages from MOZART Version 2 model [Horowitz *et al.*, 2003].

^cCalculated using Kettle *et al.* [1999] and ACE-2 measurements; see section 2.4.2 and Appendix B.

^dCalculated using methodology by B. Lamb (given by Bates *et al.* [1992]); see section 2.4.2.

^eBased on EDGAR Version 3.2 [Olivier *et al.*, 2002] and GEIA 1985 [Benkovitz *et al.*, 1996].

their provenance are summarized in Table 2. The earlier version of the model was described by Benkovitz *et al.* [1994]; changes in Version 2 are described here.

2.1. Meteorological Data

[11] The meteorological data used were obtained from the *European Centre for Medium-Range Weather Forecasts (ECMWF)* [2003]. Quantities used were the 6-hour instantaneous values from the initialized analysis surface fields (two dimensional (2-D)) and model-level fields (3-D) except for precipitation, heat fluxes, and thermal radiation, which were the accumulated 6-hour values from the gridded 12-, 18-, 24-, and 30-hour forecasts at the same resolution. The effects of the ECMWF model spin-up on the precipitation, heat fluxes, and thermal radiation values were minimized by using the 1200 UT daily forecasts and adding the forecast hour to the date to find the new date; for example, values from the 12-, 18-, 24-, and 30-hour fore-

casts on 6 June at 1200 UT were used for 7 June at 0000 UT, 0600 UT, 1200 UT, and 1800 UT (K. Fielding, European Centre for Medium-Range Weather Forecasts, personal communication, 1999). For the simulations reported here the model domain extends from 0° to 360° longitude and from the equator to 81°N with 1° resolution (approximately 111 × 111 km at the equator and 56 × 111 km at 60° latitude) and 27 levels from the surface to ~100 hPa.

2.1.1. Height of the Mixed Layer

[12] Estimates of the height of the mixed layer were required to set the vertical diffusivity coefficient; these estimates must account for differences over land and ocean areas and for the diurnal cycle of this parameter. In Version 1 the mixed layer heights had been set to a constant seasonal value; in Version 2 time- and location-dependent mixed layer heights were calculated by a multistep approach based on the equivalent potential temperature θ_e , the saturation equivalent potential temperature θ_{es} , the dew point T_d , and the height (above ground) of the model vertical levels as detailed in Appendix A. The algorithm developed captures the major global features expected in the mixed layer height (Figure 2), such as a general increase in height over the oceans from the poles to the tropics, relatively lower height

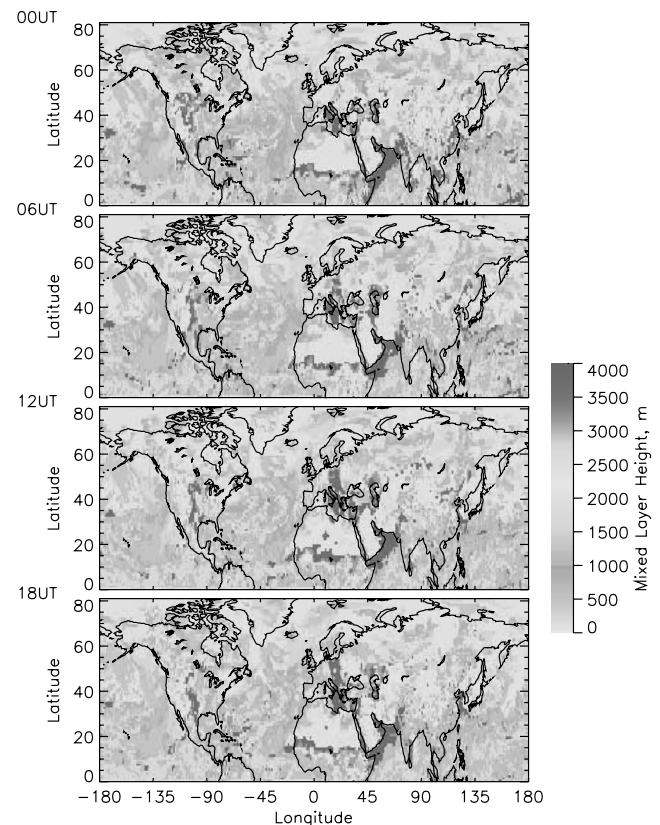


Figure 2. Heights of the mixed layer for 29 June 1997. Note the general increase in height over the oceans from the poles to the tropics, the relatively lower depths over regions of ocean upwelling such as off the coast of California, and the clear diurnal cycle particularly over land (for example, the European continent shows relatively lower height over the entire region at 0000 UT compared to 1200 UT). See color version of this figure at back of this issue.

over regions of ocean upwelling such as off the coast of California, and a clear diurnal cycle, particularly over land.

2.1.2. Vertical Diffusivity Coefficient

[13] The default value for the vertical diffusivity coefficient K_{zz} was set to $10 \text{ m}^2 \text{ s}^{-1}$ [Ko and Sze, 1991; Louis, 1979; Pasquill, 1976]. If the value of the K number, defined as $K = K_{zz}\Delta t/(\Delta z)^2$ [Brasseur and Madronich, 1992], where Δt is the transport time step and Δz is the thickness of the model level, was greater than 0.5 the value of K_{zz} was adjusted so that the K number was less than or equal to 0.5. Above the mixed layer, vertical diffusion was assumed to be negligible compared to other transport processes, so values of K_{zz} were set to zero.

2.2. Chemistry

2.2.1. Chemical Mechanisms

[14] The model represents aqueous-phase oxidation of SO_2 to sulfate by H_2O_2 and O_3 , OH- induced gas-phase oxidation of SO_2 to sulfate and of DMS to SO_2 and MSA, and gas-phase production of H_2O_2 from HO_2 . Version 1 of the model incorporated all the sulfate present into cloud water and used the limiting reagent formulation for the reaction of SO_2 with H_2O_2 ; in the current version the incorporation of sulfate into cloud water and the extent of aqueous phase oxidation of SO_2 are explicitly calculated.

[15] Aqueous-phase oxidation is calculated for all clouds for which the liquid water volume fraction (LWVF) was equal to or greater than 10^{-9} . The fraction of sulfate that is in the aqueous phase (i.e., cloud drops) is important for both the cloud water pH and the sulfate wet removal. Subgrid variability of clouds was accounted for by incorporating the sulfate into cloud water according to the LWVF as follows:

$$f_r = \frac{f_{\max} \left(\frac{L}{L_{\text{mid}}} \right)}{1 + \frac{L}{L_{\text{mid}}}}$$

where f_r is the fraction of sulfate aerosol that is incorporated into cloud water, f_{\max} is the maximum fraction of sulfate that is incorporated into cloud water, L is the grid-cell-averaged liquid water volume fraction, and L_{mid} was the liquid water volume fraction corresponding to $0.5f_{\max}$. A value of 0.5 was used for f_{\max} based on ten Brink *et al.* [1987], Daum *et al.* [1984], and Leitch *et al.* [1983], who examined aircraft measurements of the composition of cloud liquid water, interstitial air, and associated clear air to estimate the fraction of unscavenged sulfate aerosol. A value of 10^{-7} was used for L_{mid} ; the resulting uptake function is shown in Figure 3. Cloud water pH was estimated assuming that sulfate was present entirely as ammonium bisulfate and that MSA was fully dissociated; pH was constrained to be between 2.0 and 5.6. Kinetics of the aqueous-phase oxidation of SO_2 by H_2O_2 and O_3 were explicitly represented. Expressions for the temperature- and pH-dependent Henry's law coefficients and dissociation constants for the absorption of gaseous SO_2 in water were taken from Goldberg and Parker [1985]. Expressions for the temperature-dependent Henry's law coefficient of H_2O_2 and O_3 are taken from Easter and Luecken [1988]. For the oxidation by H_2O_2 the second-order expression is taken

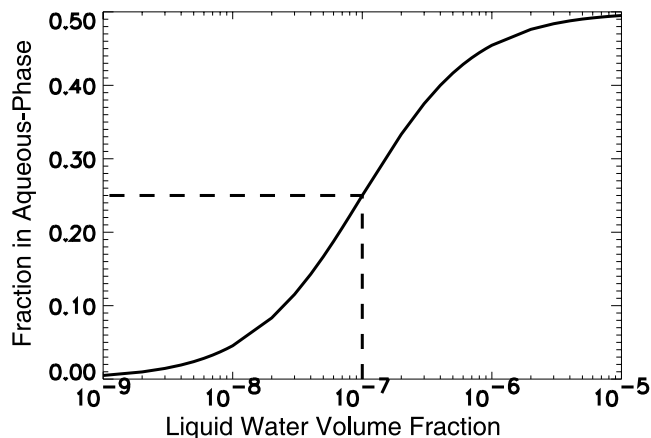


Figure 3. Fractional incorporation of sulfate into cloud water. This mechanism is activated only when cloud liquid water volume fraction is $>10^{-9}$. Dashed lines indicate the values of L_{mid} and $0.5f_{\max}$ (see section 2.2.1).

from Schwartz [1988], based on Overton [1985]. For the oxidation by O_3 the second-order expression is taken from Schwartz [1988], who used the rate coefficients of Hoigné *et al.* [1985] with temperature adjustments from Erickson *et al.* [1977].

2.2.2. Oxidant Mixing Ratios

[16] Mixing ratios of oxidant species HO_2 , H_2O_2 , O_3 and OH were based on monthly average MRs for June and July calculated using Version 2 of the Model of Ozone and Related Chemical Tracers, (MOZART) [Brasseur *et al.*, 1998; Horowitz *et al.*, 2003] driven by a GCM, the NCAR Community Climate Model. MOZART is a global model with 2.8° resolution in longitude and latitude and 25 vertical levels from 992 to 5 hPa. Anthropogenic emissions used in the MOZART simulation were taken from the EDGAR Version 2 inventory [Olivier *et al.*, 1996], which represents emissions circa 1990, with some modifications based on preliminary values from the EDGAR Version 3 inventory [Olivier and Berdowski, 2001]; biogenic emissions were based on the work of Guenther *et al.* [1995], Müller [1992], and Yienger and Levy [1995]; oceanic emissions were modified values from the inventory by Brasseur *et al.* [1998]; lightning emissions were based on the parameterizations of Price *et al.* [1997] and Pickering *et al.* [1998].

[17] As the daily average MRs generated by MOZART were obtained using a CTM driven by a GCM, the oxidant MRs are representative of typical conditions as opposed to specific meteorological situations. The day-to-day variability in the MOZART oxidant MRs was eliminated, but the geographic distribution preserved, by averaging the MRs over the June–July modeling period at each location and level of the MOZART model. The resulting averages exhibited somewhat high OH MRs over the continents, with maxima of about $6 \times 10^6 \text{ cm}^{-3}$. The grid-to-grid conversion was performed as follows. Each horizontal GChM-O grid cell was located within the larger MOZART grid, followed by linear interpolation between the lowest and highest MOZART vertical levels to the GChM-O vertical levels. The value of the lowest MOZART level was used for all the GChM-O levels within the lowest MOZART level. The hourly MRs for HO_2 and OH were

obtained as the product of the average values and the cosine of the solar zenith angle for each location and time.

[18] H_2O_2 is included in the model as an advected species formed by the reaction $2\text{HO}_2 \rightarrow \text{H}_2\text{O}_2 + (\text{O}_2)$; the values of the rate constant for this reaction were taken from *Stockwell* [1995] and *DeMore et al.* [1997]. H_2O_2 is removed by aqueous-phase oxidation of SO_2 and by wet and dry deposition; because sinks of H_2O_2 via photolysis, reaction with OH, and below-cloud scavenging were not explicitly represented, these were taken into account by not allowing the H_2O_2 MRs to exceed values obtained by the MOZART model.

2.3. Wet Removal

[19] Wet removal of sulfate and MSA incorporated in cloud water was represented by an exponential function:

$$f_k = e^{-\frac{P\Delta t}{B} \frac{W_k}{W_{\max}}}$$

where f_k is the fraction of aerosol remaining in the aqueous phase at vertical level k after model time step Δt (seconds), P is the precipitation rate at the surface ($\text{mol m}^{-2} \text{s}^{-1}$), B is the total column cloud liquid water content (LWC, mol m^{-2}), W_k is the cloud LWC at vertical level k , and W_{\max} is the maximum cloud LWC in the column. The factor W_k/W_{\max} accounts for the greater rate of precipitation formation at higher cloud LWC.

2.4. Emissions

2.4.1. Anthropogenic Emissions of SO_2 and Primary Sulfate

[20] Anthropogenic emissions of SO_2 were taken from the Emission Database for Global Atmospheric Research (EDGAR) Version 3.2 [*Olivier et al.*, 2002] inventory, which represents annual emissions circa year 1995. Seasonal emissions and breakdown between release points below and above 100 m were calculated using the appropriate fractions from the GEIA Version 1B inventory [*Benkovitz et al.*, 1996]; emissions for the Northern Hemisphere summer were used. Primary sulfate emissions for 1997 were estimated by extrapolation from the GEIA inventory as 1% of the sulfur emissions for industrialized regions (North America, Europe) and 2% for the rest of the model domain. Vertically resolved SO_2 emissions from aircraft have not yet been developed for EDGAR V3.2, so the vertically resolved aircraft emissions from EDGAR V2, which were representative of circa 1990, were adjusted according to the ratio of the total global emissions of the Version 3.2 and Version 2 inventories (J. G. J. Olivier, National Institute for Public Health and the Environment, personal communication, 2003). Aircraft emissions were assigned to the appropriate GChM-O vertical level and were assumed to have no seasonal pattern. Anthropogenic emissions, assumed to be constant over the simulation period, are presented in Figure 4a. A logarithmic scale of over 3 orders of magnitude is used to encompass the wide range of emissions density. Anthropogenic emissions were divided into three main geographic regions and the sulfate and SO_2 MRs were tracked separately for each region. The areas of high anthropogenic emissions in North America (190° – 330° , 21.1% of anthropogenic emissions), Europe (330° – 60° , 33.3% of anthropogenic emissions), and Asia

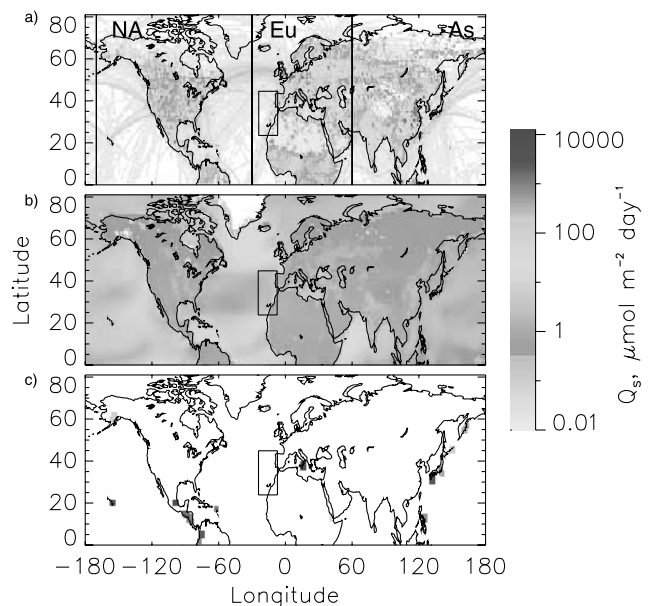


Figure 4. Sulfur emissions for the simulation period: (a) anthropogenic sources, (b) average biogenic sources, and (c) average volcanic sources. All panels use the scale shown. Volcanic emissions were divided by the area of the model grid cell where the volcano is located. The vertical lines in Figure 4a delimit the anthropogenic source regions distinguished in the model, North America (NA), Europe (Eu), and Asia (As). The rectangle delimits the ACE-2 experimental area (25° – 8°W longitude; 23° – 44°N latitude). See color version of this figure at back of this issue.

(60° – 190° , 45.6% of anthropogenic emissions) are evident in the figure; emissions over the oceans originate from ships and aircraft.

2.4.2. Biogenic Emissions

[21] Sea surface DMS concentrations from *Kettle et al.* [1999] were combined with seawater DMS measurements made during the ACE-2 field campaign to calculate time- and location-dependent oceanic DMS emissions using the wind speed transfer velocity relationship of *Liss and Merlivat* [1986], as described in Appendix B. Seasonal emissions of DMS and H_2S from land sources were calculated using the methodology of B. Lamb [*Bates et al.*, 1992] gridded to $1^\circ \times 1^\circ$ resolution [*Benkovitz et al.*, 1994]; these emissions were treated entirely as DMS in the model. Average biogenic emissions are presented in Figure 4b. Overall, biogenic emissions were significantly smaller and much more uniform spatially than anthropogenic emissions, with emissions from the ocean predominating. The high-productivity areas in the North Atlantic south of Greenland and in the tropics south of 30°N are evident in Figure 4b.

2.4.3. Volcanic Emissions

[22] Volcanic emissions are quite variable temporally and there were substantial volcanic events during the modeling period, so as far as possible daily sulfur emissions from volcanos were specific to the simulation period. The principal sources of time-specific information were the Volcano Activity Reports compiled by the Global Volcanism Program of the Smithsonian Institution and available at web

Table 3. Information on Volcano Emissions Used in the Model^a

Volcano	Latitude	Longitude	Height, ^b km	Emissions, Gg S	Country	Method ^c	Data ^d
Popocatepetl	19.02	-98.62	5.5	259	Mexico	M	1
Etna	37.73	15.00	3.4	110	Sicily, Italy	M	2
Ruiz	4.90	-75.32	5.3	52.2	Columbia	A	3
Sakura-Jima	31.58	130.67	1.1	52.2	Japan	A	3
Pu'uO'o ^e	19.45	-155.29	0.76	42.5	Hawaii, USA	M	4
Soufrière Hills	16.70	-62.20	0.92	22.4	Montserrat Island	M	5
Masaya	11.98	-86.16	0.64	21.7	Nicaragua	A	3
Satsuma Iwojima (Kikai)	30.78	130.28	0.72	20.4	Japan	R	3
Galeras	1.22	-77.37	4.3	17.9	Columbia	A	3
Fuego	14.47	-90.88	3.8	17.6	Guatemala	A	3
SanCristobal	12.70	-87.00	1.7	16.2	Nicaragua	A	3
Mayon	13.26	123.69	2.5	14.6	Philippines	A	3
Pacaya	14.38	-90.60	2.6	14.0	Guatemala	A	3
Poas	10.20	-84.23	2.7	13.8	Costa Rica	A	3
Asama	36.40	138.53	2.6	10.2	Japan	A	3
Bulusan	12.77	124.05	1.6	10.2	Philippines	A	3
Oshima	34.73	139.38	0.76	7.4	Japan	A	3
Santa Maria	14.76	-91.55	3.8	6.3	Guatemala	A	3
Karumsky	54.05	159.43	1.5	4.9	Kamchatka, Russia	A	6
Kuju	33.08	131.25	1.8	3.8	Japan	A	3
Stromboli	38.79	15.21	0.93	3.7	Aeolian Islands, Italy	M	1
Unzen	32.75	130.30	1.4	3.6	Japan	A	3
Arenal	10.46	-84.70	1.7	3.0	Costa Rica	A	3
Bezymianny ^f	55.98	160.59	2.9	2.8	Kamchatka, Russia	A	6
Halemaumau ^f	19.45	-155.29	1.2	2.5	Hawaii, USA	M	4
Telica	12.60	-86.85	1.1	2.3	Nicaragua	A	3
Aso	32.88	131.10	1.6	2.1	Japan	A	3
Momotobo	12.42	-86.54	1.3	2.0	Nicaragua	A	3
Medvezhia	45.38	148.83	1.1	1.9	Kurile Islands, Russia	A	3
Usu	42.53	140.83	0.73	1.5	Japan	A	3
Sheveluch	56.65	161.35	2.8	1.4	Russia	A	6
Augustine	59.38	-153.42	1.3	1.3	Alaska, USA	A	3
Iliamna	60.03	-153.08	3.1	0.61	Alaska, USA	A	3
Erta Ale	13.60	40.67	0.61	0.59	Ethiopia	A	3
Santa Ana	13.85	-89.63	2.4	0.55	El Salvador	A	3
Izalco	13.81	-89.63	2.0	0.55	El Salvador	A	3
Vulcano	38.4	14.96	0.5	0.37	Aeolian Islands, Italy	M	2
Kverkfjoll	64.65	-16.72	1.9	0.082	Iceland	A	3
Martin	58.17	-155.35	1.9	0.082	Alaska, USA	A	3
Total				749			

^aEmissions are totals for the simulation period (1 June to 24 July 1997).

^bHeight of volcano cone.

^cMethod: M, measurements for some days, linear interpolation for days with no measurements; R, range of emissions (random number used to generate daily emissions); A, constant 25-year average degassing (e).

^dData: 1, H. Delgado (Universidad Nacional Autónoma de México, Coyoacán, Mexico, personal communication, 1999); 2, T. Caltabiano (Istituto Internazionale di Vulcanologia, Catania, Italy, personal communication, 1999); 3, *Andres and Kasgnoc* [1998]; 4, *Elias et al.* [1998]; 5, P. Francis (deceased) (Open University, Milton Keynes, UK, personal communication, 1998); 6, P. Kyle (New Mexico Institute of Mining and Technology, New Mexico, USA, personal communication, 1999).

^eVent of Kilauea volcano, Hawaii, USA.

^fMain crater of Kilauea volcano, Hawaii, USA.

site <http://www.volcano.si.edu/gvp/gvn/index.htm> (accessed in spring 1999) and personal communication with the principal investigators conducting measurements at individual volcanos (Table 3). As most measurement schedules were not daily, daily emissions were estimated using linear interpolation (P. Francis, Open University, personal communication, 1998). In the absence of specific information for continuously degassing volcanos, the 25-year average emission rates from *Andres and Kasgnoc* [1998] were used. In the model volcanic emissions were treated entirely as SO₂.

[23] Because emissions from Karumsky (Kamchatka Peninsula), Satsuma Iwojima (Kikai, Japan), and Vulcano (Italy) were obtained as minimum and maximum values for periods of several days, daily emissions were estimated using a random function within the given minimum, maximum

range. No information was available on the status of Apoyo (Nicaragua), Concepción (Nicaragua), and Hakkoda (Japan) so emissions from these volcanos were taken as zero. None of the active volcanos was located within the ACE-2 experimental area; the closest volcanos were Etna in Sicily and Stromboli and Vulcano in the Aeolian (Lipari) Islands at distances of ~2900 km.

[24] The model injects emissions from volcanos into the atmosphere starting at the height of the cone of each volcano and extending up to four additional levels, depending on the amount of the emissions at a particular time period. At each level the fraction of the emissions injected was taken as proportional to the density of air at that level. The two largest volcano emitters during the modeling period were Popocatepetl near Mexico City and Etna in Sicily. Approximately 30% of the volcano emissions were

Table 4. Contributions of Source Regions and Source Types to Sulfur Emissions and Burdens

Source Region	Emissions, Tg S			Burden ^c			
	Eight-Week ^a	Year ^b	Percent	Sulfate		SO ₂	
				Gg S	Percent	Gg S	Percent
All sources	11.2	73		597		197	
Anthropogenic	9.0	58	80	502	84	160	81
North America	1.9	12	17	92	15	28	14
Europe	3.0	20	27	193	32	64	33
Asia	4.1	27	36	218	37	68	34
Volcanic	0.7	5	7	63	10	27	14
Biogenic	1.5	10	13	32	5	10	5

^aTotal emissions for the eight-week simulation period.

^bEmissions extended to year to facilitate comparison with other studies.

^cAverage over six-week analysis period.

released at heights less than 2000 m, ~26% between 2000 and 4000 m, and ~44% over 4000 m. Only three volcanos account for the emissions released at heights greater than 4000 m: Popocatepetl (Mexico, 5465 m), Ruiz (Colombia, 5321 m), and Galeras (Columbia, 4276 m).

[25] Approximately 59% of the sulfur emissions from volcanos were based on measurements combined with interpolations, 38% were 25-year averages assumed constant for the simulation period and 3% were based on information on minimum/maximum emissions. Information on the volcanos active during the experimental period is presented in Table 3, and average emissions for the simulation period are presented in Figure 4c.

2.4.4. Assessment of Emissions Values

[26] Sulfur emissions in the model domain were dominated by anthropogenic sources; these sources contributed ~80% of the sulfur emissions, biogenic sources contributed ~13%, and volcanos contributed ~6%. The distribution of emissions by source region and source type for the eight-week simulation period and extended to one year is presented in Table 4; Asian sources were the largest contributors to both the total and the anthropogenic emissions.

[27] As 1995 anthropogenic emissions were used in a 1997 simulation, the impact of this was assessed using information obtained from regional agencies in Europe and North America. In Europe, emissions data are reported by participants to the Convention on Long-Range Transboundary Air Pollution (CLRTAP) to the United Nations Economic Commission for Europe/Co-operative Programme for Monitoring and Evaluation of Long Range Transmission of Air Pollutants in Europe (UNECE/EMEP); in addition, expert estimates by the Meteorological Synthesizing Centre–West (MSC-W) of EMEP are also developed to supplement the reported data and for use in EMEP modeling work [Vestreng and Klein, 2002]. Total emissions of SO₂ in the EMEP European domain were estimated to be 16.3 Tg S in 1995 and 14.4 Tg S in 1997, ~12% decrease; the largest reductions were in Germany and the United Kingdom. In the United States the U.S. Environmental Protection Agency estimates yearly emissions using a “bottom-up” methodology [U.S. Environmental Protection Agency, 2000]. The difference between emissions in 1995 and 1997 was calculated using emissions by state obtained from the U.S. Environmental Protection Agency web site Tier Emissions Report–Criteria Air Pollutants at <http://www.epa.gov/air/data/nettier.html?us~usa~United%20States>. Total emissions

of SO₂ in the United States were estimated to be 8.6 Tg S in 1995 and 8.8 Tg S in 1997, ~1.5% increase.

[28] In Asia, sulfur emissions have been increasing in the 1990s and estimates have larger uncertainty because of poorly developed regional emission factors and lack of accurate knowledge of the sulfur contents of the fuels used. *Streets et al.* [2000, 2001] estimated SO₂ emissions in Asia to be 19.2 Tg S in 1995 and 19.6 Tg S in 1997, ~2% increase. The country-based estimates developed by different investigators agreed to between 15% and 20% [Benkovitz et al., 2004], and regional estimates agreed to ~4%, except for the EDGAR estimate of the Asian total which is ~28% higher than estimates from regional investigators.

[29] Because most anthropogenic emissions were due to the combustion of fossil fuels, a relatively small uncertainty of ±30% had been placed on the global annual average [Lelieveld et al., 1997]; however, this uncertainty increases when the combustion of biofuels and biomass burning are included in anthropogenic emissions totals. Currently no reliable new quantitative values of the uncertainty are available, although these values are thought to be well in excess of the 1995–1997 differences in the inventories for the several source regions.

[30] Although the error in the annual global mean oceanic DMS surface concentrations has been estimated at ±50% [Penner et al., 2001], the error in the seasonal and regional concentrations can be up to a factor of 5; these errors are compounded by differences in air/sea flux parameterizations, which can in turn add a factor of 2 difference to the estimates of DMS emissions from the ocean [Kettle and Andreae, 2000]. However, at locations where biogenic emissions are much smaller than anthropogenic emissions, the uncertainty in the biogenic emissions would not be a large input to the uncertainty in the total emissions.

[31] Total volcanic sulfur emissions for the eight-week simulation period were 0.75 Tg, which corresponds to annual emissions of ~4.5 Tg. This estimate is comparable to the global estimates for continuous emissions presented in Table 1b of Mather et al. [2003], ~3 to ~5 Tg yr⁻¹, the global estimate of 3.5 Tg S yr⁻¹ for noneruptive volcanos by Spiro et al. [1992], and the estimate of 10 Tg yr⁻¹ in the Northern Hemisphere by Graf et al. [1997]. Differences in these estimates can be accounted for by the methodologies used to estimate the emissions, by the different domains covered in some of the estimates, by the intermittent nature and great discrepancies in the estimates of emissions from both degassing and eruptive events, and because measurement values used in this study were selected to represent, as much as a possible, the time period of the simulation.

3. Observations

[32] Model results were evaluated using measurements taken during the simulation period, mainly by monitoring networks; summary information on the networks and measurements is presented in Table 5. The spatial area used for evaluation is a model grid cell (1° × 1°), referred to as a location, and model vertical level. Stations were assigned to a location on the basis of their latitude and longitude; for each observation the model vertical level was selected according to the station altitude and the height of the model levels at the time of observation. Where concurrent mea-

Table 5. Information on the Measurements Used to Evaluate Model Results

Network Area	Number		Measurements	Sampling Intervals	Data Provider	Percent Observations
	Stations	Observations				
ACE-2 ^a short-term	2	57	SO ₂ (several) ^b	semicontinuous	IGAC ^c	0.2
ACE-2 ^a short-term	7	183	sulfate (several) ^b	semicontinuous	IGAC ^c	3.0
ABPM ^d Canada	7	14	wet deposition	twice per month	Nat/Chem ^c	0.6
AEROCE ^e oceanic	4	116	sulfate (24 hours)	every day	D. Savoie ^g	1.9
AIRMoN ^h USA	8	34	sulfate	every week	Nat/Chem ^c	0.6
AIRMoN ^h USA	9	76	wet deposition	every week	Nat/Chem ^c	3.2
AIRS ⁱ USA	597	16,655	SO ₂ (1 hour) ^b	continuous	V. Ambrose ^j	68.8
AIRS ⁱ USA	192	1334	sulfate (24 hours)	every sixth day	V. Ambrose ^j	22.0
BCPCSN ^k Canada	4	15	wet deposition	every week	Nat/Chem ^c	0.6
CAPMoN ^l Canada	10	332	SO ₂ (24 hours)	every day	Nat/Chem ^c	1.4
CAPMoN ^l Canada	10	352	sulfate (24 hours)	every day	Nat/Chem ^c	5.8
CAPMoN ^l Canada	21	340	wet deposition	every day	Nat/Chem ^c	14.4
CASTNet ^m USA	69	330	SO ₂ (7 days)	every week	Nat/Chem ^c	1.4
CASTNet ^m USA	67	327	sulfate (7 days)	every week	Nat/Chem ^c	5.4
CASTNet ^m USA	19	78	wet deposition	every week	Nat/Chem ^c	3.3
EMEP ⁿ Europe	82	2511	SO ₂ (24 hours)	every day	A.-G. Hjellbrekke ^o	10.4
EMEP ⁿ Europe	78	2805	sulfate (24 hours)	every day	A.-G. Hjellbrekke ^o	46.2
EMEP ⁿ Europe	77	924	wet deposition	event	A.-G. Hjellbrekke ^o	39.0
GAViM ^p Canada	3	33	sulfate (24 hours)	every third day	Nat/Chem ^c	0.5
IMPROVE ^q USA	7	67	SO ₂ (24 hours)	2 days/week	K. Perry ^r	0.3
IMPROVE ^q USA	64	647	sulfate (24 hours)	2 days/week	K. Perry ^r	10.7
NADP ^s USA	179	681	wet deposition	weekly	NADP web site ^t	28.8
NAPS ^u Canada	55	1635	SO ₂ (24 hours)	every day	Nat/Chem ^c	6.8
NAPS ^u Canada	32	160	sulfate (24 hours)	every sixth day	Nat/Chem ^c	2.6
NBPMN ^v Canada	13	61	wet deposition	every week	Nat/Chem ^c	2.6
NEPMoN ^w Canada	2	8	wet deposition	every week		0.3
NSPSN ^x Canada	1	15	wet deposition	every day	Nat/Chem ^c	0.6
NYST ^y USA	2	59	SO ₂ (24 hours)	every day	L. Husain ^z	0.2
NYST ^y USA	2	64	sulfate (24 hours)	every day	L. Husain ^z	1.0
REPQ ^{aa} Canada	37	154	wet deposition	weekly	Nat/Chem ^c	6.5
Cheju Island, Korea	1	38	SO ₂ (1 hour) ^b	continuous	Y. P. Kim ^{bb}	0.2
Cheju Island, Korea	1	12	sulfate (48 hours)	every third day	C. H. Kang ^{cc}	0.2
Taiwan	69	2509	SO ₂ (1 hour) ^b	continuous	C. M. Liu ^{dd}	10.4

^aAerosol Characterization Experiment 2 (ACE-2).

^bMeasurements averaged to 24 hours for comparison with observations.

^cInternational Global Atmospheric Chemistry Program (IGAC) ACE-2 data sets.

^dAlberta Precipitation Monitoring Network.

^eThe Canadian National Atmospheric Chemistry (Nat/Chem) Database and Analysis System [Ro and Vet, 2002].

^fAerosol Oceanic Chemistry Experiment.

^gUniversity of Miami, Coral Gables, Florida, USA, 2001.

^hAtmospheric Integrated Research Monitoring Network.

ⁱAerometric Information Retrieval System.

^jU.S. Environmental Protection Agency, Research Triangle Park, North Carolina, USA, 2000.

^kBritish Columbia Precipitation Chemistry Sampling Network.

^lCanadian Air and Precipitation Monitoring Network.

^mClean Air Status and Trends Network.

ⁿEuropean Modeling and Evaluation Programme Network.

^oNorwegian Institute for Air Research, Kjeller, Norway, 2000.

^pGuelph Aerosol and Visibility Monitoring Program.

^qInteragency Monitoring of Protected Visual Environments.

^rSan Jose State University, San Jose, California, USA, 2000.

^sNational Atmospheric Deposition Network.

^t<http://nadp.sws.uiuc.edu>.

^uNational Air Pollution Surveillance Network.

^vNew Brunswick Precipitation Monitoring Network.

^wNewfoundland Acid Precipitation Monitoring Network.

^xNova Scotia Precipitation Study Network.

^yNew York State Department of Health stations at Whiteface Mountain and Mayville, New York.

^zNew York State Department of Health, Albany, New York, USA, 2000.

^{aa}Reseau d'Echantillonnage des Precipitations du Quebec.

^{bb}Korea Institute of Science and Technology, Seoul, Korea, 2000.

^{cc}Cheju University, Cheju, Korea, 2000.

^{dd}National Taiwan University, Taipei, Taiwan, 2000.

measurements were available at multiple stations within a location, these were averaged to obtain the observed MRs; each pair of modeled and observed MRs at a location, vertical level, and date is referred to as a case. Concurrent observations at a location and vertical level permitted

examination of intralocation variability due to subgrid variability and/or measurement error.

[33] Sulfate and SO₂ measurements used were made by routine air quality monitoring networks in North America, Europe, and Taiwan and stations in the Canary Islands and

Korea. If necessary, reported concentrations were converted from the original units to MRs in units of ppb; observations reported at station temperature and pressure were converted to MRs using the ECMWF meteorological data. Sampling start and stop times based on local time were converted to Universal Time (UT) to permit comparisons with modeled MRs. Observed MRs corrected for sea salt sulfate were used in these evaluations. A summary of the data sets is presented in Appendix C; maps of the evaluation locations are presented in Figure 5.

4. Evaluation of Model Results and Observations

[34] A general concern with the accuracy of results obtained with CTMs driven by analyzed meteorological fields is the accuracy of values of these fields; any inaccuracy in transport parameters or in cloud and precipitation amounts and/or locations directly influences the model results. Thus even if all the aerosol processes were accurately represented in the model, errors in the meteorological fields would degrade the evaluations between modeled and observed values; consequently any departure reflects inaccuracy both in the representation of the processes in the model and in the meteorological fields that drive the CTM. Especially important are the three-dimensional field of cloud presence and the two-dimensional fields of cloud fraction and precipitation amount, which are difficult to accurately represent in numerical weather prediction models [Jung and Tompkins, 2003; Mullen and Buizza, 2001]. In the present model the nonreanalyzed 1997 ECMWF data were used; these forecasts overestimated the precipitation amount, although subsequent changes in the model resolution and physical parameterizations starting in 1999 have gone a long way toward correcting the overestimation [Cherubini et al., 2001; Lalauette et al., 2003]. Errors in these fields directly influence both the principal mechanism of sulfate formation, aqueous-phase conversion of SO_2 to sulfate, and the principal sink of aerosol sulfate, wet deposition. In addition, any errors in wind speed and direction and/or times, locations and amounts of cloud and precipitation fields result in temporal and spatial displacements of modeled values with respect to the observations, which degrade point-to-point evaluations. If such displacements could be taken into account, evaluation results would improve, and examination of residual errors might refine understanding of representation of chemical and scavenging processes. These considerations suggest the utility of additional tools, such as visualization and pattern recognition techniques, to enhance the utility of model-observation evaluations. An initial step in this direction, taken here, is comparison of time series at specific locations, in which temporal displacement becomes readily apparent.

4.1. Time Series of Sulfate and SO_2 Mixing Ratios

[35] Time series of the modeled and observed sulfate MRs at all 90 locations for which sulfate was measured on at least 28 of the 38 analysis days are shown in Figure 6. The model accurately reflected the spatial distribution of sulfate; in general locations with small observed MRs exhibited small modeled MRs and vice versa. In addition, almost all locations displayed good agreement in episodicity (patterns of short-term temporal variability) and quite a few displayed

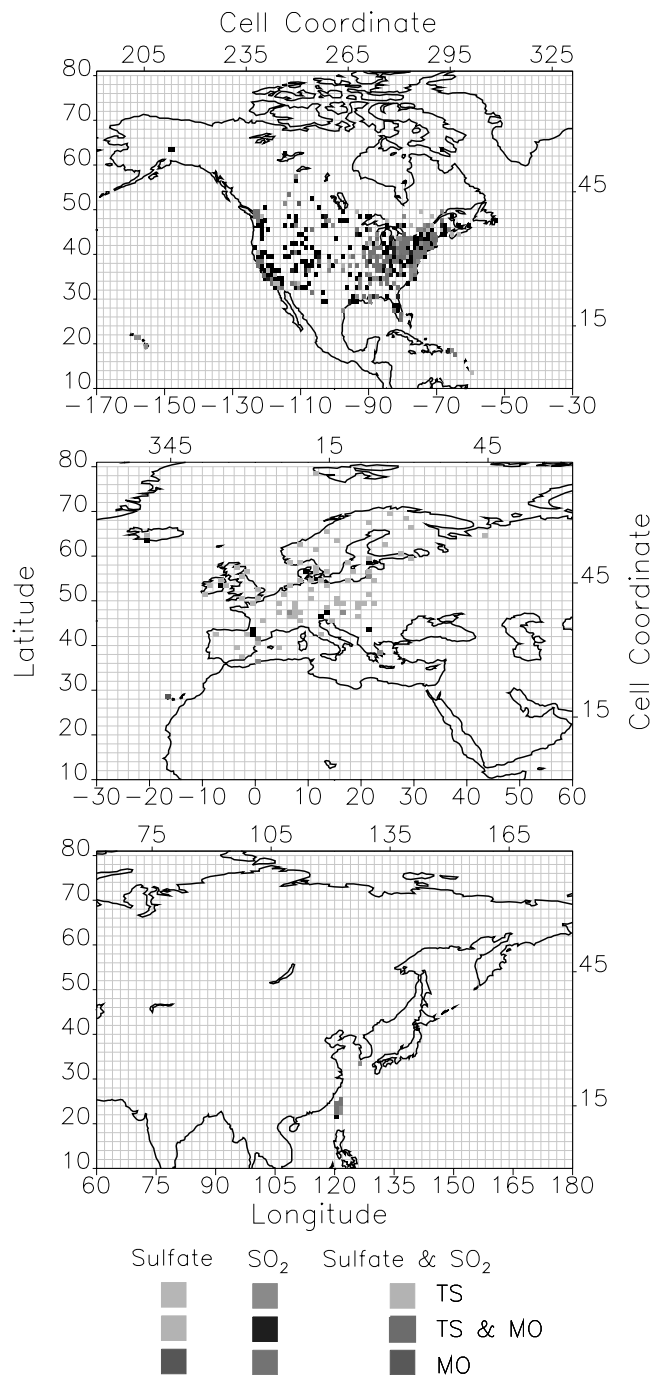


Figure 5. Map of the evaluation locations for sulfate and SO_2 . TS denotes locations for which time series data were available, and MO denotes locations at which there were multiple observations. See color version of this figure at back of this issue.

good agreement in magnitude, with locations in source regions exhibiting the greatest discrepancies in magnitude and sometimes in episodicity. There were several instances of remarkably good quantitative agreement, for example, locations in Norway (8, 58, 0), Denmark (10, 54, 0), Sweden (17, 58, 0), Great Britain (353, 54, 0), and Spain (358, 42, 0); the notation by which the locations are labeled is explained in Figure 7. Examples of agreement in episodicity, but not

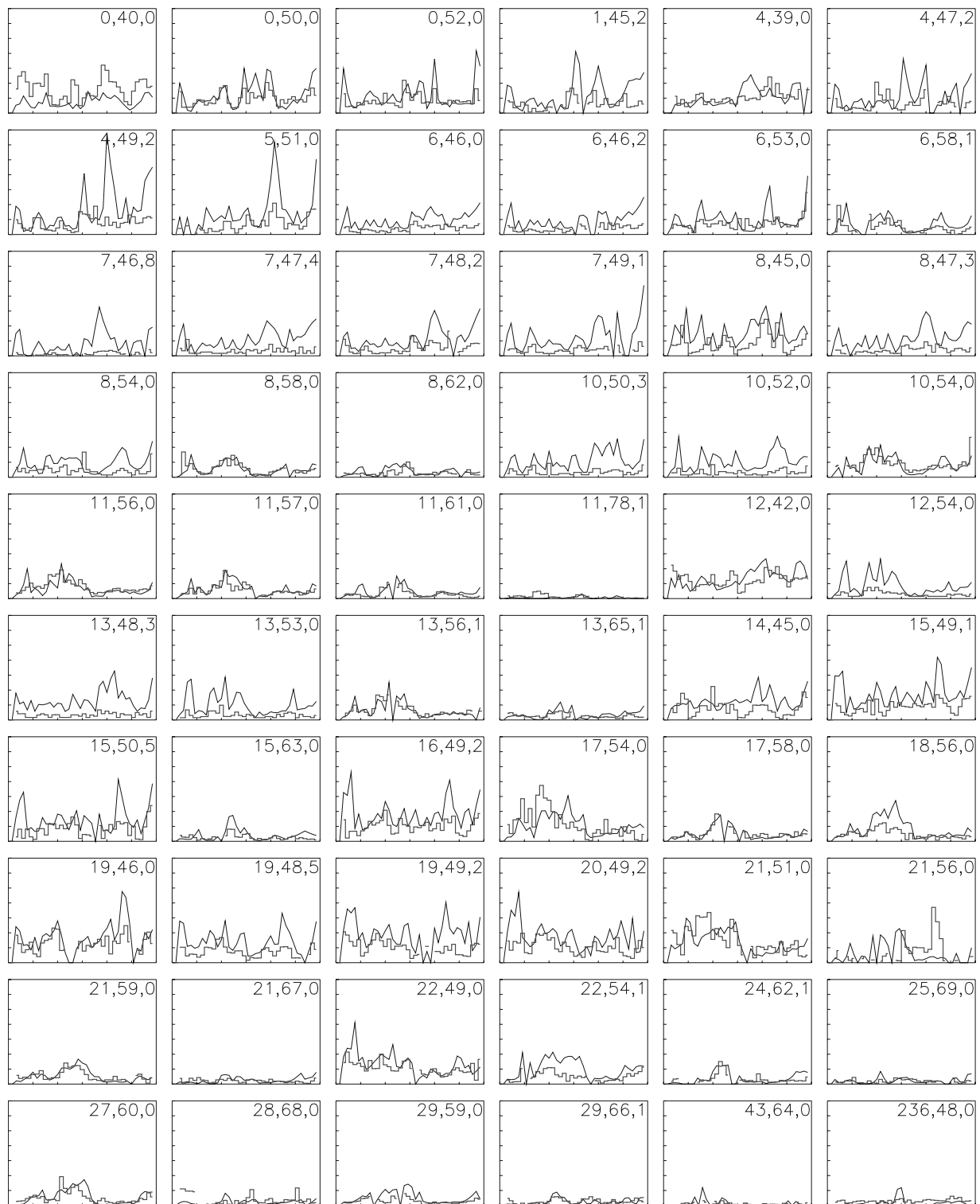


Figure 6. Time series of the modeled and observed sulfate mixing ratios at the 90 locations that had at least 28 observations for the period 17 June to 24 July 1997. The three numbers, i, j, k , at the top right of each panel represent the three-dimensional model coordinates of the location. Model domain is numbered east from the prime meridian (0–360) and north from the equator (0–81), and vertical levels are numbered from the surface. See color version of this figure at back of this issue.

as good agreement in magnitude, were locations in Slovakia (19, 49, 2) and Canada (282, 46, 0) and (294, 44, 0). Examples of temporal displacement of modeled values were locations in Poland (17, 54, 0) and Latvia (21, 56, 0).

Locations (8, 58, 0), (10, 54, 0), (21, 56, 0), and (17, 58, 0) were in northern Europe, in areas not impacted directly by SO_2 emissions from central Europe; locations (353, 54, 0), and (358, 42, 0) were in western Europe upwind from areas

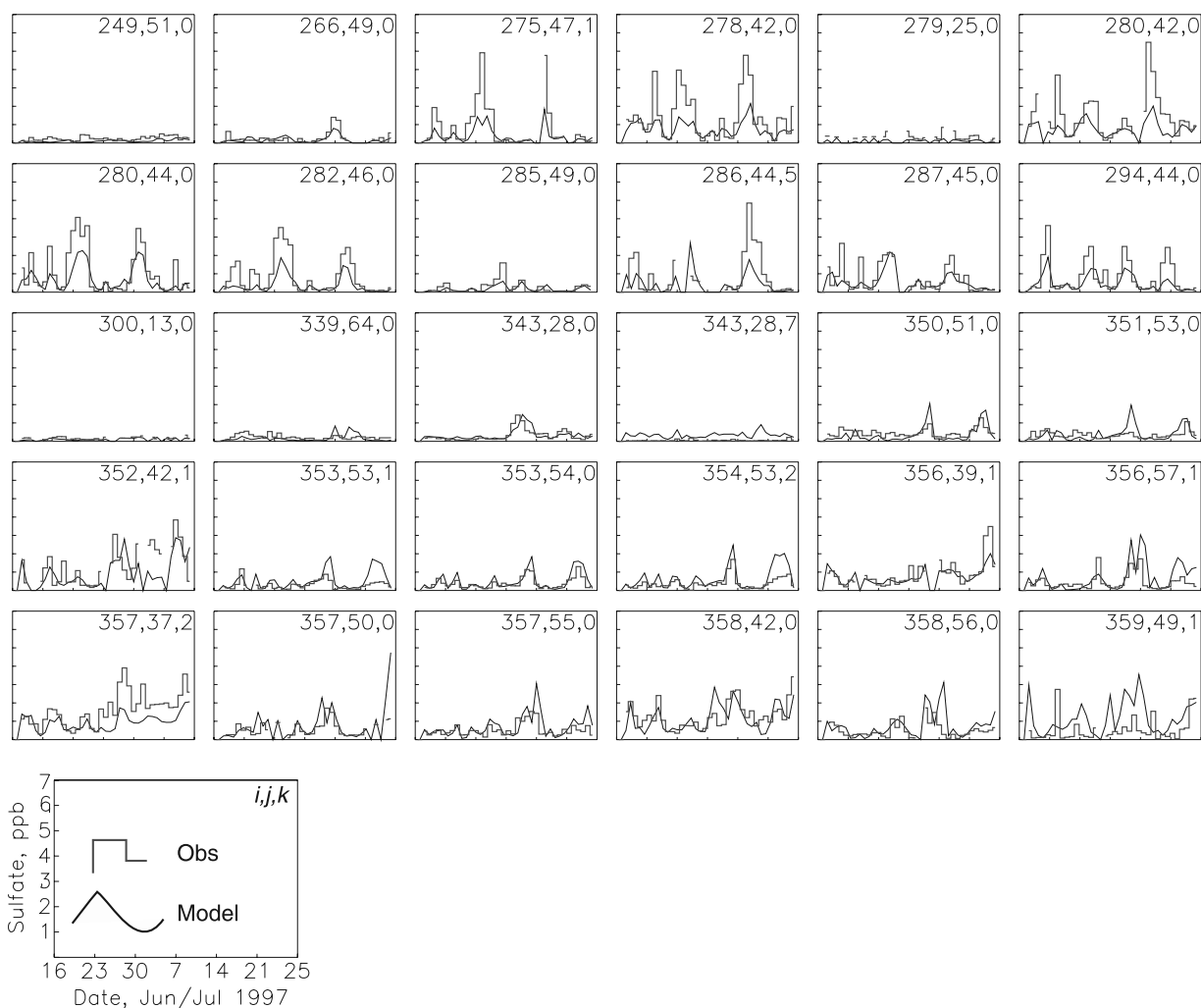


Figure 6. (continued)

of high SO_2 emissions. Locations (17, 54, 0) and (19, 49, 2) were in areas of high SO_2 emissions in central Europe; locations (282, 46, 0) and (294, 44, 0) were downwind from areas of high emissions in North America.

[36] The high temporal and spatial variability of SO_2 lead to mixed results in the time series analysis. Figure 7 presents SO_2 time series at four of the 274 locations available for this analysis. At a location in Taiwan (120, 22) the modeled MRs were within the scatter of the observed MRs; however, the model mostly overestimated the average MRs. Another location in Taiwan (120, 24) presents an example of extreme spatial inhomogeneity; the single station with high observed MRs sufficiently influenced the average observed MRs that model results substantially underestimated the average MRs. A location in Georgia, United States (269, 38), presents an example of good agreement between modeled and average observed MRs and a location in New Hampshire, United States (287, 43), presents an example of the consequences of setting an artificial lower limit to reported quantities.

4.2. Quantitative Evaluation of Sulfate and SO_2 Mixing Ratios

[37] In over half the cases ($\sim 56\%$), modeled sulfate MRs were within a factor of 2 of the observed MRs, and $\sim 77\%$

of the modeled MRs were within a factor of 3 (Figure 8a). The distribution of modeled and observed values is almost symmetrical below and above the 1:1 line; for example, MR_m/MR_o was between 1 and 2 in 27.0% of the cases and between 0.5 and 1 in 28.5% of the cases, with similar results for the other ranges. SO_2 modeled and observed MRs exhibited somewhat greater departure (Figure 8b) with $\sim 39\%$ of the ratios within a factor of 2 and $\sim 56\%$ within a factor of 3, and the distribution of the ratios of modeled to observed values was skewed toward values greater than 1. For MRs averaged over the whole 38-day simulation (similar to monthly averages commonly reported), the factor of 2 and factor of 3 percentages increased to 65.3% and 90.0% for sulfate and to 45.5% and 59.8% for SO_2 ; the improved agreement between model values and averaged observations illustrates how model evaluations using longer time periods tend to smooth over differences between modeled and observed values. As model errors may be masked by the longer averaging period, a more stringent evaluation of model performance is obtained by comparisons at fine temporal resolution.

[38] The model performance was quantitatively evaluated by examination of the differences between modeled and observed MRs and the ratio characteristic spread. Histo-

grams of $MR_m - MR_o$, classified by the observed value (Figure 9), permit assessment of model bias. For both sulfate and SO_2 the distributions peaked at a low value of this difference and were reasonably symmetric about zero, indicative of a lack of bias of the model. As the peaks in the distributions include a wide range of observed MRs, not just small values, the model accuracy indicated by the histogram

is not just a consequence of small differences when observed MRs are small. Approximately 52% of the sulfate observations and $\sim 59\%$ of the SO_2 observations were overestimated by the model.

[39] The ratio characteristic spread S used in this work is a measure of the ratios of MRs [Benkovitz and Schwartz, 1997]. A study by McNair *et al.* [1996] concluded that the spatial variability in observed pollutant concentrations within model grid cells should be taken into account in developing performance guidelines for model evaluation. For evaluation of two observed MRs, $S_{o/o}$, or for evaluation of modeled and observed MR, $S_{m/o}$, S is defined as the ratio of the greater MR to the lesser MR. For more than two observed MRs this definition is generalized as $S_{o/o} = \exp[2s.d.(\ln MR_o)]$ and $S_{m/o} = \exp[|\ln(MR_m/\overline{MR_o})|]$, where MR_o is the observed MR, MR_m is the modeled MR, s.d. is the standard deviation, and $\overline{MR_o}$ is the average of the observed MRs. As a measure of the spread of the observed MRs due to analytical uncertainties, different measurement techniques, sampling protocols, and/or sub-grid variation, the spread of multiple observations within a single grid cell for a single observation period, $S_{o/o}$, is a measure of the best agreement that might be expected between modeled and observed MRs. Thus multiple observed MRs at different sites within individual model grid cells are needed to assess the expected agreement.

[40] For sulfate the distributions of $S_{o/o}$ and $S_{m/o}$ for the multiple observations set (Figures 10a and 10b) were similar, but somewhat broader for $S_{m/o}$, with median values of 1.33 for $S_{o/o}$ and 1.66 for $S_{m/o}$. The relative contribution of each observed MR range to each range of S was similar between the two distributions, with comparable fractions exhibiting values of S greater than 5. Of the 1.66 value of $S_{m/o}$ 1.33 was attributed to subgrid variation and/or measurement error and a comparable amount was attributed to model error. The distribution of $S_{m/o}$ for the entire data set (Figure 10c) was broader than for the multiple observations set, with a median value of 1.85 and a greater fraction of the cases with $S_{m/o}$ values greater than 5. The relative contributions of each observed MR range to each $S_{m/o}$ range were impacted mainly by the differences in the relative fractions of cases where the observed MRs were less than 0.33 ppb and greater than 3 ppb. The larger value of $S_{m/o}$ for the entire data set may be due to subgrid variability not being captured by a single monitoring station, and/or to greater measurement or model error at smaller MRs.

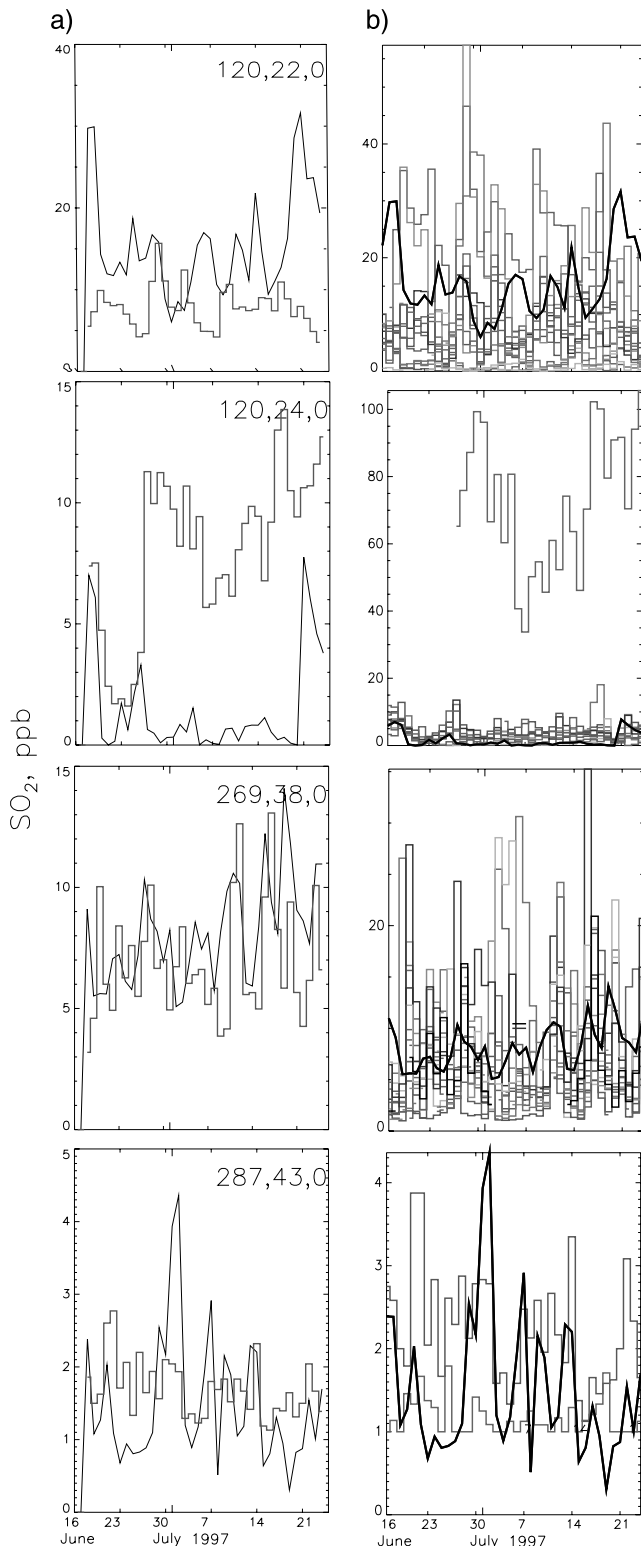


Figure 7. Examples of time series of SO_2 at locations with more than one station. Each horizontal pair of panels represents one model grid cell; the three numbers, x, y, z , at the top right of the left panel represent the three-dimensional model coordinates (i, j, k) of the location. In all panels the black lines represent the model results. In Figure 7a the cityscape red lines represent the average of all the observed mixing ratios. In Figure 7b the cityscape lines represent observed mixing ratios at individual stations within the model grid cell; the vertical spread of these lines on a given date represents the within-location spatial variability of the mixing ratios on that date. Note the artificial lower limit for reporting the observed mixing ratios for one station in the last panel. See color version of this figure at back of this issue.

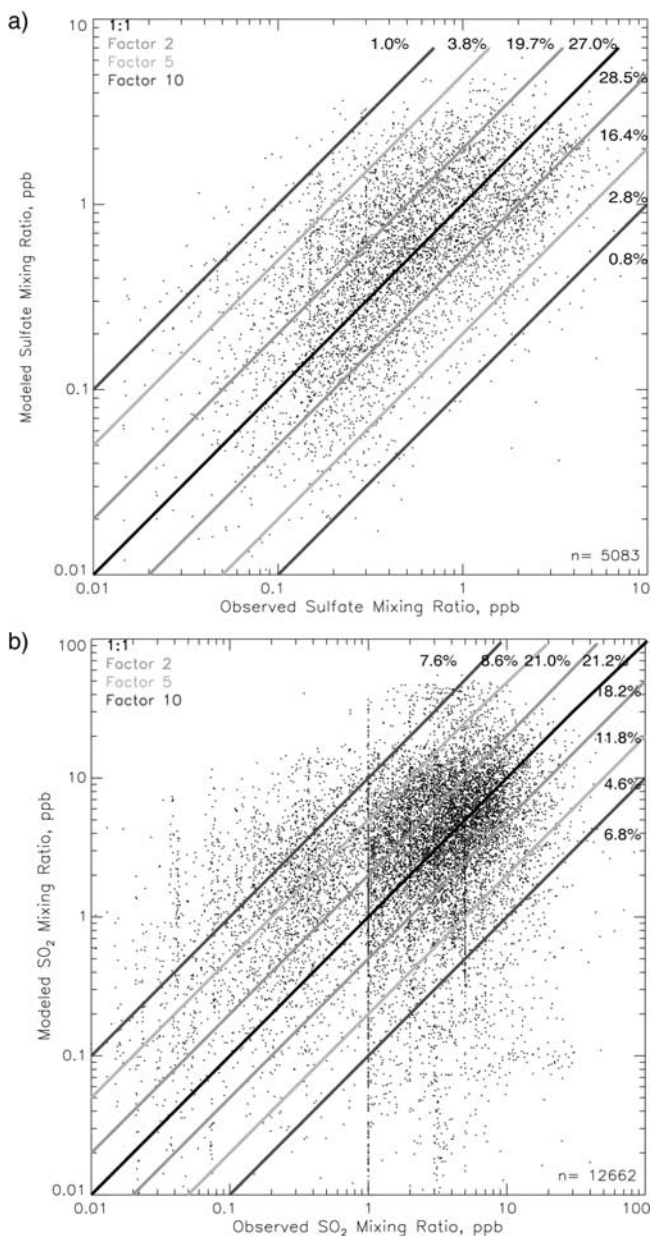


Figure 8. Scatterplots of modeled versus observed mixing ratios of (a) sulfate and (b) SO₂. Here, *n* indicates the number of cases in each plot. Observed SO₂ MRs in a straight line, especially evident at 1 ppb, were caused by an artificial setting of the lower limit of reporting for measurements; this is further illustrated in Figure 7. See color version of this figure at back of this issue.

[41] For SO₂ the distribution of *S*_{o/o} (Figure 10d) is broader than that of *S*_{m/o} (Figure 10e), with median values of 2.32 and 1.87, respectively. Measured SO₂ MRs can have great temporal and spatial variability within individual locations, as shown by *Benkovitz et al.* [1994] and in

Figure 9. Histograms of the differences between modeled and observed values classified by the values of the observation (a) sulfate mixing ratios, (b) SO₂ mixing ratios, and (c) sulfate concentration in precipitation.

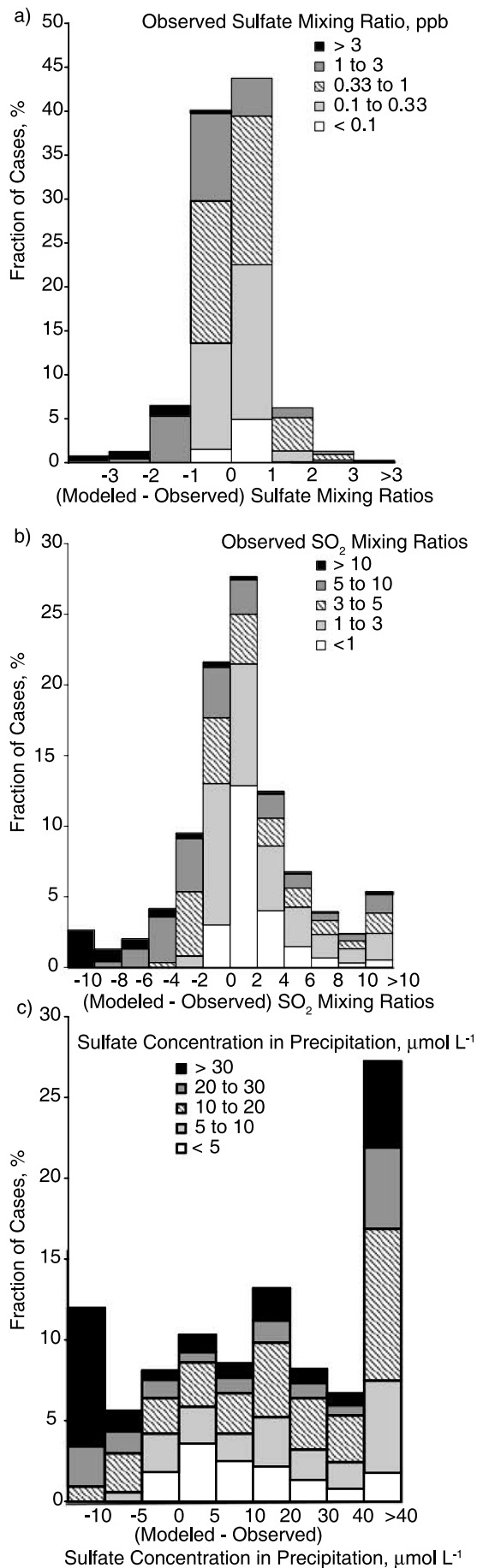


Figure 7; the narrower distribution and smaller median value of $S_{m/o}$ compared to $S_{o/o}$ could be a result of averaging the measurements to obtain the observed MRs used in the model evaluation. The relative contribution of each observation range to each category was similar between the two distributions, and the fraction of the evaluations with S values greater than 8 is approximately the same for both. The median value of $S_{m/o}$ for the entire data set was 2.55, a large fraction attributable to the high degree of within-location spatial variation evident from the median value of $S_{o/o}$. The distribution of $S_{m/o}$ (Figure 10f) was similar to but broader than that of $S_{m/o}$ for the multiple observations set, with the relative contributions of each observed MR range to each $S_{m/o}$ range impacted mainly by the differences in the relative fractions of cases where the observed MRs were less than 1 ppb. Values of $S_{m/o}$ exceeded 8 in approximately 17% of the evaluations; of these approximately 1.4% were from locations for which more than 50% of the $S_{m/o}$ values were greater than 8, but only $\sim 16\%$ of the locations with larger discrepancies had multiple observations. Locations with more than 50% of their $S_{m/o}$ values greater than 8 were in the larger emissions areas of central and eastern Europe, where most of the modeled MRs were overestimated (possibly because of overestimated SO_2 emissions), and a few locations in western North America where most of the modeled MRs were underestimated, possibly because of subgrid variability not being appropriately captured or because of spatial and/or temporal displacement errors.

4.3. Quantitative Evaluation of Sulfate Concentration in Precipitation

[42] In contrast to sulfate MRs, for which little model bias was exhibited, there was considerable bias in the modeled concentrations of sulfate in precipitation, with $\sim 74\%$ of the observed concentrations overestimated by the model. All of the observed concentrations less than $5 \mu\text{mol L}^{-1}$ were overestimated, and $\sim 34\%$ of the observed concentrations in the range of $10\text{--}20 \mu\text{mol L}^{-1}$ were overestimated (Figure 9c). Approximately 45% of the modeled concentrations were within $10 \mu\text{mol L}^{-1}$ of the observed concentrations, and $\sim 27\%$ of the differences between modeled and observed concentrations were greater than $40 \mu\text{mol L}^{-1}$.

[43] For the observed sulfate concentration in precipitation approximately 29% of the concurrent measurements locations had stations separated by 10 km or less with a median distance of ~ 40 km; this may account for the high percentage of $S_{o/o}$ values less than or equal to 1.5 (Figure 10g). For the multiple observation data set the distribution $S_{o/o}$ was much narrower than that of $S_{m/o}$ (Figures 10g and 10h), with median values of 1.36 and 2.44, respectively. Values of $S_{o/o}$ exceeded 6 only for observed concentrations in the $10\text{--}20 \mu\text{mol L}^{-1}$ range, whereas the $S_{m/o}$ values greater than 6 included observations from all ranges. The median value of $S_{m/o}$ for the whole data set was 2.82 (Figure 10i), slightly higher than that for the multiple data set, with $\sim 17\%$ of the cases having $S_{m/o}$ values greater than 8; of these $\sim 8.5\%$ were from locations that had more than 50% of the $S_{m/o}$ values greater than 8, but only $\sim 18\%$ of the locations with large discrepancies had multiple observations (usually two stations). Only two locations with $S_{m/o}$ values greater than 8 were located in Europe and in both the concentrations were underestimated; the rest of the locations were in North America where

most of the concentrations were overestimated in areas with large emissions (eastern half, larger precipitation) and underestimated in areas with smaller emissions (western half, smaller precipitation).

[44] Analyses of concurrent observations within a model grid cell ($S_{o/o}$) and of the modeled and observed MRs ($S_{m/o}$) with fine temporal resolution demonstrate that the model represents the observed sulfate and SO_2 MRs with an accuracy comparable to the spatial variability and measurement error of the observed MRs. These analyses demonstrate the need for concurrent multiple measurements at locations where substantial subgrid variability is expected (for example, those within or close to major emissions regions) to adequately capture this variability and thus allow more accurate evaluations of model results. These analyses also demonstrate the importance of driving the model with meteorological quantities and other model input data representing as accurately as possible the conditions at the time when the observations were made.

5. Discussion

[45] Quantities such as contributions of source regions to emissions and to sulfate burdens, turnover times (mean residence time, τ) and removal rates (inverse τ , τ^{-1}) for both sulfate and SO_2 , and the yields for aerosol sulfate and MSA are some of the measures of the performance of a model which may be compared to other estimates of these quantities, and which can be used in simpler models and for studies such as those that estimate sulfate radiative forcing [Charlson *et al.*, 1992; Haywood and Shine, 1995]. Despite the fact that the present model may not represent a “steady state” system and the geographic domain was not completely “closed,” it is nonetheless possible to estimate these key budget quantities on the basis of the model results. Material flowed out of the south, the north and the top boundaries of the model domain, although transport across the equator is known to be slow in comparison with removal rates, and MRs at the northern and top boundaries were small. For the six-week analysis period the sulfate outflow (flow out of the domain) averaged between $\sim 2\%$ of the total sinks for North American sources and $\sim 5\%$ for volcanic sources; SO_2 outflow averaged less than 1% except for volcanic sources for which it was less than 2%. Volcanic sources have the most outflow because the largest emitting volcano, Popocatepetl, is located near the southern border of the model domain. Sulfate formed in the aqueous phase and deposited in the same event did not contribute to atmospheric aerosol sulfate; therefore these amounts were not included in calculations of aerosol sulfate yields and turnover times. As discussed by Benkovitz *et al.* [1994] the following calculations were based on burdens and sink rates. For sulfate and MSA sinks were wet and dry deposition; for SO_2 sinks were chemical conversion, and wet and dry deposition. Estimates of turnover times and removal rates for any given species were calculated as $\tau = \int B dt / \int S dt$, where B is the burden (mol) and S is the sink rate (mol h^{-1}) in the domain integrated over the analysis period; the sink rate does not include the outflow material. The sulfate and MSA yields were calculated as $y = \int C dt / \int S dt$ where C is the chemical conversion rate of SO_2 to sulfate or DMS to MSA (mol h^{-1}), respectively, in the domain integrated over the analysis period.

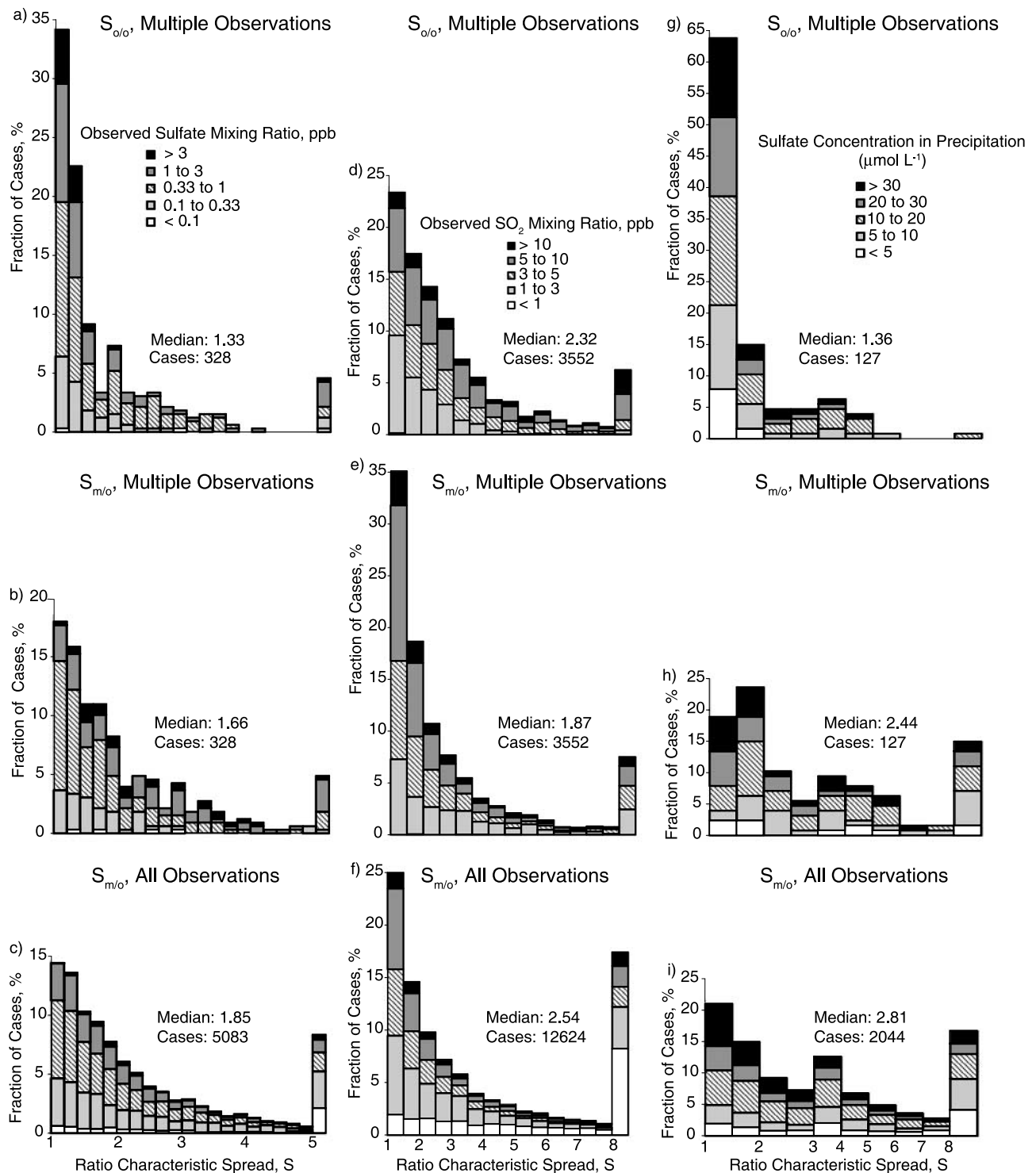


Figure 10. Histograms of the distribution of the ratio characteristic spread. (a) Characteristic spread of the observed sulfate mixing ratios within individual locations, (b) characteristic spread of model and observed sulfate mixing ratios for the data set included in Figure 10a, and (c) characteristic spread of all modeled and observed sulfate mixing ratios. (d) Characteristic spread of the observed SO_2 mixing ratios within individual locations, (e) characteristic spread of model and observed SO_2 mixing ratios for the data set included in Figure 10d, and (f) characteristic spread of all modeled and observed SO_2 mixing ratios. (g) Characteristic spread of the observed sulfate concentration in precipitation within individual locations, (h) characteristic spread of model and observed sulfate concentration in precipitation for the data set included in Figure 10g, and (i) characteristic spread of all modeled and observed sulfate concentration in precipitation.

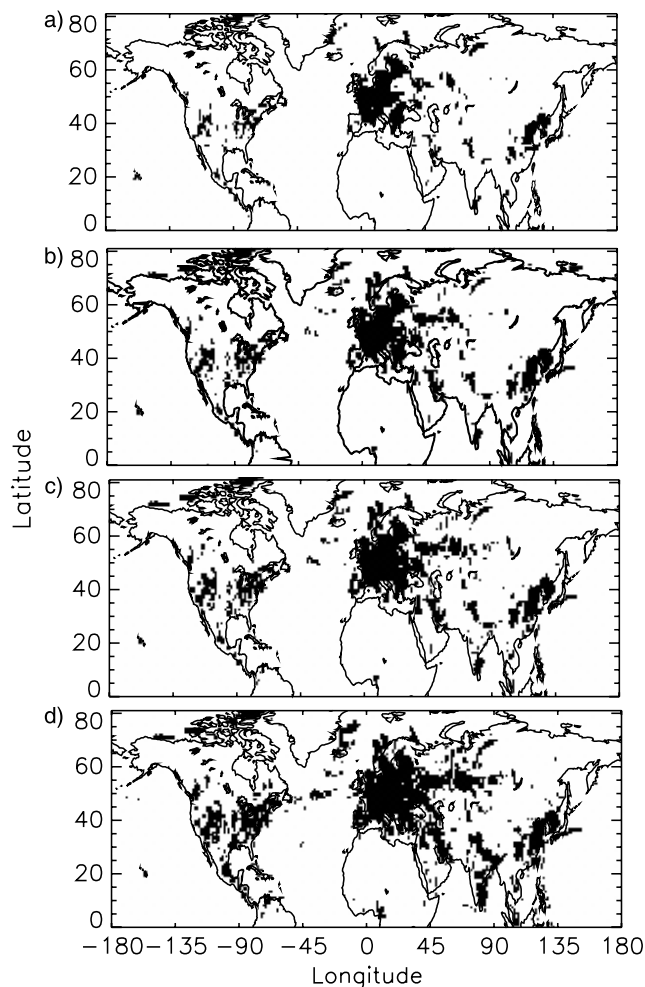


Figure 11. Areas where the SO_2 mixing ratios are greater than the H_2O_2 mixing ratios on 6 July 1997 at 0000 UT for model level (average height, m) (a) 4 (789), (b) 3 (478), (c) 2 (232), and (d) 1 (65).

[46] Aqueous-phase oxidation of SO_2 by H_2O_2 is the principal mechanism for the generation of sulfate. Therefore, for each source region and source type, the fraction of SO_2 in areas where the SO_2 MR was less than the H_2O_2 MR and the fraction of SO_2 that encountered clouds are key factors in the relative importance of sulfate generation mechanisms and of the SO_2 sinks. The domain-average fraction of SO_2 located in areas where the SO_2 MR was less than the H_2O_2 MR was calculated as

$$\overline{F_{\text{SO}_2}} = \frac{\sum_{ij} A \sum_k f c_{\text{SO}_2} \Delta h_k}{\sum_{ij} A \sum_k c_{\text{SO}_2} \Delta h_k},$$

where A is the area of the grid cell (m^2), f is equal to one if the SO_2 MR is less than the H_2O_2 MR and equal to zero otherwise, c is the SO_2 concentration (mol m^{-3}), and Δh_k is the depth of model level k (meters). The SO_2 MR was greater than the H_2O_2 MR mainly over large anthropogenic source areas (Figure 11). These areas extended to higher model levels over Europe and central Asia because $\sim 49\%$

of the emissions from European sources were emitted into the second model level, as compared to $\sim 39\%$ for Asian sources and $\sim 35\%$ for North American sources. The extent of these areas over North America and Asia decreased considerably above the second model level; above this level the areas were located mainly over heavily industrialized sections of the United States and China and mountainous regions of Central America (for example, Mexico City, a large source, is located at a height of 2240 m). Because the MRs of SO_2 from biogenic sources were considerably less than the H_2O_2 MRs, the time series of the fraction of SO_2 in areas where SO_2 was less than H_2O_2 for this source type showed little variability over time; however, the large day-to-day variability in volcanic emissions resulted in a large variability in the time series of this fraction for volcanic sources.

[47] The domain-average fraction of SO_2 or sulfate in clouds was calculated as

$$\overline{F_{\text{cl}}} = \frac{\sum_{ij} f_c A \sum_k f c_{\text{sp}} \Delta h_k}{\sum_{ij} A \sum_k c_{\text{sp}} \Delta h_k},$$

where f_c is the cloud fraction for the grid cell (equal for all vertical levels), A is the area of the grid cell (m^2), f is equal to one if the LWVF was greater than 10^{-9} at vertical level k and equal to zero otherwise, c is the concentration (mol m^{-3}), sp denotes the species (SO_2 or sulfate), and Δh_k is the depth of model level k (meters). Time series of the fraction of SO_2 in clouds by source region and source type, which reflected the daily cycle of clouds, exhibited very small variability for biogenic sources but large variability for volcanic sources. The amount of sulfate that encountered precipitating clouds was calculated by setting f equal to one if LWVF was greater than 10^{-9} at vertical level k and there was precipitation in the grid cell, and equal to zero otherwise. Time series of this quantity by source region and source type, which reflected the daily cycle of precipitation, showed fairly small variability, with the largest variability exhibited by sulfate from Asian sources.

[48] Examination of the relative contributions of the SO_2 to sulfate oxidation pathways to the total sink of SO_2 and to the conversion of SO_2 to sulfate by source region and source type showed that the contribution of the aqueous-phase oxidation was the largest and the contribution of the gas-phase oxidation was the smallest for biogenic sources (Table 6). Almost all of the SO_2 from biogenic emissions ($\sim 94\%$) was located in regions where its MR was less than that of H_2O_2 , so the large fraction of SO_2 converted via the fast aqueous-phase oxidation left a smaller fraction of the SO_2 to experience the slower gas-phase oxidation. In addition, the OH concentration in most of the areas of largest biogenic emissions (south of 20°N and north of 50°N , Figure 2) was generally smaller than over areas of largest anthropogenic and volcanic emissions. The contribution of the aqueous-phase oxidation to the total conversion of SO_2 to sulfate for biogenic SO_2 was the largest of all source types. The release heights of volcanic emissions were much higher than those for anthropogenic and biogenic emissions; thus the SO_2 from this source type was much less subject to dry deposition and the contribution

Table 6. SO₂ Sinks, Amount of SO₂ in Areas Where the SO₂ Mixing Ratio is Less Than the H₂O₂ Mixing Ratio, and Amount of SO₂ in Cloud by Source Region and Source Type^a

Source Region	Sinks (Percent of Sources)						F_{aq} , %	F_{SO_2} , ^b %	F_{cl} , ^c %
	Aq-Conv Aerosol	Reactive Rainout	Total Aq-Conv	Gas-Conv	Dry Dep				
All	33	23	56	16	27	67	45	13	
North America	32	28	60	13	27	71	56	9	
Europe	32	18	50	19	31	63	48	12	
Asia	34	22	56	15	29	69	33	14	
Volcanic	34	32	66	30	6	53	40	15	
Biogenic	39	29	68	10	22	80	94	12	

^a“Aq-Conv” aerosol is the aqueous-phase generated sulfate that contributes to aerosol burden. “Reactive rainout” is the aqueous-phase sulfate generated and deposited in same event. “Total Aq-Conv” is the total aqueous-phase conversion (aq-conv aerosol plus reactive rainout). Dep, deposition. F_{aq} , the fraction of SO₂ converted to aerosol sulfate by aqueous-phase oxidation, was calculated as the amount of SO₂ converted to aerosol sulfate via aqueous-phase conversion divided by the amount of SO₂ converted to aerosol sulfate via aqueous- and gas-phase conversion. Wet deposition is less than 0.01% of the SO₂ sinks for all source regions and source types.

^bTime- and domain-average fraction of SO₂ located in areas where SO₂ mixing ratios are less than or equal to H₂O₂ mixing ratios (see section 5 for details).

^cTime- and domain-average fraction of SO₂ located in clouds with cloud liquid water fraction $\geq 10^{-9}$ (see section 5 for details).

of this sink to the total SO₂ sinks was the smallest of all source types. The smaller dry deposition rate allowed greater time for the conversion of SO₂ to sulfate by both conversion pathways; for this source type the contribution of the gas-phase oxidation to the total SO₂ sinks was the largest and the contribution of the aqueous-phase sink was the second largest; however, because of the large gas-phase conversion (a factor of 2 or more greater than for other source types) the contribution of the aqueous-phase oxidation to the total conversion of SO₂ to sulfate was the smallest of all sources.

[49] The fraction of SO₂ in areas where the SO₂ MR was less than the H₂O₂ MR ranged from 56.1% for North American sources to 32.7% for Asian sources. The larger fraction for North American sources was the result of the HO₂ distribution, which showed larger concentrations over North America, especially over the eastern United States and Canada, coinciding with areas of largest emissions from these sources. The relative importance of the total aqueous-phase oxidation to the total sinks of SO₂ and to the conversion of SO₂ to sulfate is the result of a tradeoff between the relative amounts of SO₂ and H₂O₂ and the fraction of SO₂ in clouds. The greater fraction of SO₂ from North American sources in areas where the MR of SO₂ was less than the MR of H₂O₂ appears to have compensated for the smaller fraction of SO₂ in clouds, so the contribution of the aqueous-phase oxidation to the total SO₂ sinks was largest of all anthropogenic sources. The greater fraction of SO₂ in clouds for Asian sources appears to have compensated for the smaller fraction of SO₂ in areas where the MR of SO₂ was less than the MR of H₂O₂, so the contribution of the aqueous-phase oxidation to the total SO₂ sinks for this source region was the lowest for all anthropogenic sources.

[50] Turnover times for modeled SO₂ varied between 0.7 days for biogenic SO₂ and 2.2 days for volcanic SO₂ (Table 7). Biogenic SO₂ had the shortest turnover time

because ~94% of this SO₂ was located in areas where the SO₂ MRs were less than the H₂O₂ MRs (Table 6), resulting in rapid conversion of SO₂ to sulfate. Volcanic SO₂ had the longest turnover time because the elevated release height of these emissions reduced their exposure to dry deposition. For anthropogenic emissions the relative length of the turnover time was a result of a tradeoff between the relative amounts of SO₂ and H₂O₂ and the fraction of SO₂ in clouds in an analogous way to the influence on the relative importance of the total aqueous-phase oxidation to the total sinks of SO₂ as discussed above.

[51] Turnover times for modeled sulfate (Table 8) varied between ~4 days for sulfate from biogenic emissions to ~9 days for sulfate from volcano emissions; the overall turnover time for all sulfate was ~7 days. Wet deposition is the major sink for sulfate, so there appears to be an inverse relation between turnover time and the fraction of sulfate encountering precipitating clouds for each source region and source type. Volcanic (biogenic) sources have the longest (shortest) turnover time and the smallest (largest) fraction of sulfate encountering precipitating clouds. For anthropogenic emissions European sources have the longest turnover time and the smallest fraction of sulfate encountering precipitation clouds. These results may be compared to analyses of atmospheric measurements of natural and bomb test radioactive species, which can be used as surrogates for accumulation mode aerosol particles, inferred turnover times of 5 to 10 days [Chamberlain, 1991];

Table 7. Effective First-Order Removal Rates τ^{-1} and Turnover Times τ for SO₂ and DMS

Source Region	τ^{-1} , % d ⁻¹			Total	τ , days
	Dry Deposition	OH Conversion	Aqueous Conversion		
All	24	14	51	89	1.1
North America	30	14	67	111	0.9
Europe	25	15	39	79	1.2
Asia	29	14	57	100	1.0
Volcanic	3	13	29	45	2.2
Biogenic SO ₂	32	15	102	149	0.7
Biogenic DMS		99		99	1.0

Table 8. Effective First-Order Removal Rates τ^{-1} and Turnover Times τ for Aerosol Sulfate and MSA, Yields of Aerosol Sulfate (Fraction of SO_2 That Is Oxidized to Aerosol Sulfate) and MSA (Fraction of DMS That Is Oxidized to MSA), Aerosol Sulfate Burden/Sulfur Sources, Sulfate Sinks, and Amount of Sulfate Encountering Precipitating Clouds

Source Region	τ^{-1} , % d ⁻¹			τ , days	Aerosol Yield, %	Sulfate (or MSA) Potential, ^a days	Sinks (% Total)		$F_{\text{cl.}}^{\text{b}}$ %
	Dry Dep	Wet Dep	Total				Wet Dep	Dry Dep	
All	1.6	13	15	6.9	50	3.4	89	11	10.7
North America	1.7	14	15	6.5	45	2.9	89	11	10.9
Europe	2.0	11	13	7.9	50	3.7	84	16	9.0
Asia	1.4	14	15	6.4	49	3.2	91	9	11.9
Volcanic	1.0	10	11	9.0	64	5.2	92	8	8.7
Biogenic SO_4	2.2	21	23	4.3	49	2.2	91	9	15.9
Biogenic MSA	3.3	22	25	3.9	11	0.3	87	13	

^aSulfate potential is the sulfate burden divided by the sulfur emissions. Sulfate potential for biogenic sources is the biogenic sulfate burden divided by the biogenic SO_2 . MSA potential is MSA burden divided by DMS emissions.

^bTime- and domain-average fraction of sulfate in precipitating clouds with cloud liquid water fraction $\geq 10^{-9}$ (see section 5 for details).

analyses of measurements of the decay of atmospheric concentrations of ^{137}Cs in the weeks following the Chernobyl accident inferred turnover times of 7 to 9 days [Cambray *et al.*, 1987].

[52] The results presented here, which include analyses in three dimensions, may be contrasted with those of Koch *et al.* [2003], who found a significant negative correlation between observed daily cloud cover and surface sulfate concentrations in Europe and North America. However, the influence of other important factors in the aqueous-phase production of sulfate, such as cloud liquid water content and the relative concentrations of SO_2 and H_2O_2 , were not included in their statistical analyses. Those investigators suggested that clouds inhibit sulfate (via inhibition of gas-phase production and scavenging by precipitation) more than they enhance it (via aqueous-phase production). Three experiments were conducted using the Goddard Institute for Space Studies general circulation model (GISS GCM) with online sulfur chemistry to consider the relative contributions of gas and aqueous-phase conversion pathways to the correlation behavior. The model did not identify the sulfate generated via aqueous-phase conversion that is rained out in the same event; if this sulfate were not included in the amount produced by this pathway the conclusion that models probably have excessive aqueous-phase generation of sulfate might need to be re-examined. A correction in the dissolved species scheme used in the model improved the correlation between clouds and surface sulfate, but resulted in a larger bias between modeled and observed surface sulfate.

[53] The relative contribution of the several source types to the sulfate burden is somewhat different from their contribution to emissions (Table 4). Whereas volcanic sources represented $\sim 6\%$ of emissions, their contribution to the sulfate burden was $\sim 10\%$; this is a consequence of the longer lifetime and higher sulfate yield. In contrast, biogenic sources contributed $\sim 13\%$ of the emissions, but only $\sim 5\%$ of the burden; this is a consequence of the shorter lifetime of sulfate from these sources. Anthropogenic sources contributed slightly less to the emissions ($\sim 80\%$) than to the sulfate burden ($\sim 84\%$). The fractional contribution of North American and Asian sources to emissions and to the sulfate burden was within $\sim 1\%$; however, because of the larger yield and longer residence time of sulfate (Table 8) from European sources, these sources contributed $\sim 5\%$ more to the burden than to the emissions. The contribution

of the several source types to the SO_2 burdens is similar to the contribution to the sulfate burden except that because of the different turnover times anthropogenic sources contribute somewhat less and volcanic sources contribute somewhat more. Volcanic emissions have the largest sulfate potential, defined [Rasch *et al.*, 2000a] as the ratio of the sulfate burden to the SO_2 emissions, by a factor of between 1.4 and 2.4 (Table 8), and biogenic emissions have the smallest; emissions from European sources have the largest ratio of all the anthropogenic emissions, and emissions from North America have the smallest. These results are driven by differences in turnover times and the importance of conversion pathways and removal mechanisms of the different source types as discussed above.

[54] On the basis of the results of the present study (which includes the period June–July 1997 only) the mean burden in the model domain (Table 4) was estimated at 0.59 Tg S for sulfate and 0.20 Tg S for SO_2 . These values must be expected to be larger for sulfate and smaller for SO_2 than those from simulations for a full year because both species exhibit a seasonal cycle (more conversion and therefore more sulfate and less SO_2 in the summer; less conversion and therefore less sulfate and more SO_2 in the winter), and are somewhat less than global values because of the limited geographic domain of the model. Feichter *et al.* [1997] estimated that 69% of the sulfate and 76% of the SO_2 are found in the Northern Hemisphere.

[55] In contrast to the study presented here, which consisted of an eight-week simulation of the Northern Hemisphere for June–July 1997 at $1^\circ \times 1^\circ$ and 27 vertical levels using meteorological information specific to those times and locations and additional model input data adjusted as much as possible to reflect the simulation period, previous modeling studies have for the most part performed global and generally multiyear simulations at coarser resolutions, some incorporated into a GCM or using output from a GCM. Two studies that presented information on the influences of source regions and/or source types on sulfate burdens are compared with results presented here. These studies both used meteorological information generated by a GCM and presented averages over several simulation years. Graf *et al.* [1997] examined the source strength of volcanic SO_2 emissions and their contribution to the global sulfate distribution using a coupled climate-chemistry GCM with 3.75° resolution in the vertical and 19 vertical levels to 10 hPa. No primary anthropogenic sulfate emissions were included, and

Table 9. Models Used for Comparisons of Lifetimes and Sinks of Sulfate and SO₂

Model	Resolution (Vertical Levels)	Meteorological Data Source	Simulation Period ^a	Oxidant Concentrations	Reference
Hamburg ECHAM GCM ^b	5.625° × 5.625° (19)	GCM	5 years	prescribed	<i>Feichter et al.</i> [1997]
Hamburg ECHAM GCM	5.625° × 5.625° (19)	GCM		<i>Roelofs and Lelieveld</i> [1995]	<i>Lelieveld et al.</i> [1997]
Hamburg ECHAM GCM	5.625° × 5.625° (19)	GCM	3 years	<i>Roelofs and Lelieveld</i> [1995]	<i>Roelofs et al.</i> [1998]
GISS GCM II-prime	4° × 5° (9)	GCM	6 years	C. Spivakovsky ^c	<i>Koch et al.</i> [1999]
NCAR/CCM3	2.8° × 2.8° (18)	GCM	7 years	IMAGES [<i>Müller and Brasseur</i> , 1995] ^d	<i>Rasch et al.</i> [2000a]
GOCART	2° × 2.5° (25)	GEOS/DAS ^e	6 years	IMAGES [<i>Müller and Brasseur</i> , 1995]	<i>Chin et al.</i> [2000a, 2000b]
CSIRO GCM	5.6° × 3.2° (18)	GCM	4 years	prescribed	<i>Rotstajn and Lohmann</i> [2002]
GChM-O Version 1	1.125° × 1.125° (15)	ECMWF ^f	June–July 1986	prescribed ^g	<i>Benkovitz et al.</i> [1994]
GChM-O Version 2	1° × 1° (27)	ECMWF	June–July 1997	MOZART [<i>Horowitz et al.</i> , 2003] ^h	this study

^aNumber of years of simulation; results were reported as averages for those years.

^bGeneral circulation model.

^cC. Spivakovsky (Harvard University, Cambridge, Massachusetts, personal communication, 1996).

^dIntermediate Model of Global Evolution of Species.

^eGoddard Earth Observing System/Data Assimilation System. Cloud fraction and cloud water content derived from empirical formulations.

^fEuropean Centre for Medium-Range Weather Forecasts.

^gH₂O₂ generated at fixed rate dependent on season. OH from C. Spivakovsky (Harvard University, Cambridge, Massachusetts, personal communication, 1990).

^hModel of Ozone and Related Chemical Tracers.

DMS was converted to SO₂ only. A three-month spin-up time was allowed, and global averages from a 5-year simulation were presented. Volcanic emissions had the largest sulfate potential (called efficiency by Graf et al.) and anthropogenic emissions the smallest, and the contribution of volcanic emissions to the sulfate burden was almost as much as the contribution from anthropogenic emissions, a much greater fraction from that found in the study presented here. Although the lack of detailed information in the Graf et al. paper precludes a full explanation of all the reasons that could account for the differences with the study presented here, several factors can be listed. In the Graf et al. study total Northern Hemisphere emissions were larger (79 Tg S yr⁻¹), the relative contributions of the various source types was different (biogenic ~9.5%, anthropogenic ~78%, volcanic ~13%) compared to values from the present study (Table 4), and the distribution of the volcanic emissions was fairly different (for example, volcanos in Iceland and the Kamchatka Peninsula had greater emissions). A large fraction of anthropogenic sources and some of the larger emitting volcanos were located in midlatitudes, where there is a strong seasonal signal in oxidant concentrations and reaction rates; in contrast, a large fraction of the biogenic sulfate is generated south of 30°N, where the seasonal signal is not as pronounced, altering the relative conversion of these emission sources depending on the season and impacting the annual values presented in their study.

[56] *Rasch et al.* [2000a] performed a study using the National Center for Atmospheric Research's GCM (Community Climate Model Version 3, CCM3) with 2.8° horizontal resolution and 18 vertical levels to 35 km. The sulfur cycle was included in the GCM, and oxidant concentrations were prescribed from fields generated in an independent run of the Intermediate Model of Global Evolution of Species (IMAGES) [*Müller and Brasseur*, 1995]. A 3-year simulation was performed with the sulfur components tagged by region of origin. In this simulation, CCM3 had several biases that directly impacted the sulfur cycle: the amplitude of the seasonal cycle of precipitation over the continental United States was larger than observations, maxima in spring and minima in late fall in precipitation over central

Europe not seen in observations, and low summertime cloud cover over continents. The two most important processes controlling sulfate were identified as the aqueous-phase conversion of SO₂ and the wet deposition sink of sulfate, both of which are highly dependent on the meteorological information on clouds and precipitation. Annual average global sulfate and SO₂ burdens were 0.60 Tg S and 0.4 Tg S, respectively. Regions denoted North America and Europe were defined in limited latitude ranges (15°–90°N for North America, 21°–90°N for Europe), and biogenic emissions were divided according to these geographic regions; thus direct comparisons with results from the present study are difficult. The emissions inventories used by Rasch et al. reflected emissions circa 1985, which included larger emissions in North America and Europe and smaller emissions in Asia than the inventory used in the study presented here, which reflected emissions circa 1995. For North American and Asian emissions the anthropogenic sulfate potential was similar in Rasch et al. and in the study presented here (Table 8); however, the sulfate potential for European emissions is significantly lower in Rasch et al. (attention is called to error in Figure 5 of Rasch et al.; the units should be Gg not Tg). There could be several reasons for this difference. European emissions were large and were located mainly north of 40°N, where the oxidant cycle has a large seasonal signal, influencing yearly averages when compared to values for a specific summer season. In addition, the strong northwest flow over Europe in June–July 1997 transported European emissions south of 21°N (an area not included in the Rasch et al. definition of the European region) where large OH concentration, sparse precipitation, and high temperatures promoted additional gas-phase oxidation of SO₂ and slower removal of sulfate.

[57] Several studies (briefly summarized in Table 9) were selected for comparison of key physical diagnostic quantities. In addition to the differences indicated in the table key processes differed in many respects among these studies, including emissions inventories, parameterizations of transport, chemical mechanisms, and wet and dry deposition. The summer simulation for June–July 1986 given by *Benkovitz and Schwartz* [1997] using Version 1 of the present model is also included. The rates of the several

Table 10. Sink Rates, Inverse Lifetimes, Lifetimes, Contributions to Sinks, Burden of SO₂ and Sulfate, and Sulfate Potential From This Study and Other Models^a

	F97	L97	R98	K99	R00	C00	R02	B97	This Study
<i>Sink Rates, % d⁻¹</i>									
SO ₂									
Dry deposition	26	10	8	17	16	26	19	12	24
Wet deposition	5	0	0	0	1	7	4	0	4 × 10 ⁻⁴
Gas conversion	11	7	8	6	6	9	6	8	14
Aqueous conversion	22	26	27	15	29	15	26	16	30 ^b
Oxidation and immediate wet deposition									21
Sulfate									
Wet deposition	3	5	5	4	2	2	2	3	2
Dry Deposition	20	14	17	14	23	15	15	18	13
<i>Inverse Lifetime, % d⁻¹</i>									
SO ₂	63	43	42	38	53	56	62	36	90
Sulfate	23	19	21	18	25	17	24	21	15
DMS	48	200		53	71	50	71	34	100
MSA				13		14		21	25
<i>Lifetime, days</i>									
SO ₂	1.6	2.3	2.4	2.6	1.9	1.8	1.6	2.8	1.1
Sulfate	4.4	5.3	4.7	5.7	4.0	5.8	4.2	4.7	7.0 ^b
DMS	2.1	0.5		1.9	1.4	2.0	1.4	2.9	1.0
MSA				7.6		7.1		4.8	3.9
<i>Sinks, %</i>									
SO ₂									
Dry deposition	42	24	18	44	31	46	35	34	27
Wet deposition	8	0	0	0.2	2	12	8	<1	4 × 10 ⁻⁴
Gas conversion	17	16	18	16	12	16	10	21	16
Aqueous conversion	34	59	64	39	56	27	47	45	56 ^c
Sulfate									
Dry deposition	14	25	22	20	7	13	12	14	11
Wet deposition	86	75	78	80	93	87	88	86	89
Sulfate yield, ^d %	51	76	82	55	68	43	57	66	50 ^b
<i>Burden, Tg S</i>									
SO ₂	0.33	0.56	0.61	0.56	0.4	0.43	0.42		0.20 ^e
Sulfate	0.43	1.05	0.96	0.73	0.60	0.63	0.67		0.60 ^e
Sulfate potential, ^f days	2.1	4.4	3.7	3.4	2.5	2.7	3.2		3.3

^aF97, *Feichter et al.* [1997]; B97, June–July 1986 simulation [*Benkovitz et al.*, 1994; *Benkovitz and Schwartz*, 1997]; L97, *Lelieveld et al.* [1997]; R98, *Roelofs et al.* [1998]; K99, *Koch et al.* [1999]; R00, *Rasch et al.* [2000a]; C00, *Chin et al.* [2000a, 2000b]; R02, *Rotstajn and Lohmann* [2002].

^bIncludes aerosol sulfate only, i.e., does not include sulfate generated and removed in the same time step.

^cIncludes 33% conversion to aerosol sulfate and 23% sulfate generated and removed in the same time step.

^dCalculated as chemical conversion rate of SO₂/sink rate of SO₂.

^eCovers only model domain; average over six-week analysis period.

^fCalculated as sulfate burden/(SO₂ burden × SO₂ inverse lifetime).

removal processes of sulfate and SO₂ for the models (Table 10) show marked model-to-model differences for key processes. For example the rates of dry deposition and aqueous-phase oxidation of SO₂ range over a factor of three. The present model exhibits the highest aqueous-phase conversion rate of the several models (51% d⁻¹); this removal process includes aqueous-phase reaction which forms sulfate that remains in the atmosphere (30% d⁻¹) and that is removed in the time step in which it is formed (reactive rainout, 21% d⁻¹); it is not clear to what extent the rate of aqueous conversion in the other models is lower because it encompasses only sulfate which remains in the atmosphere. The high aqueous-phase removal rate in the present model results in a lifetime of SO₂ (1.1 days), which is considerably shorter than values determined in previous studies (1.8 to 2.8 days, the latter value from a study using Version 1 of the present model). Certainly some of the model-to-model differences may be reflective of the different meteorological conditions and geographical domains

treated in the models; this conclusion gains support in the fact that the lifetimes of SO₂ from the several source types examined in the present model vary from 0.7 day (biogenic, Table 7) to 2.2 days (volcanic). Nonetheless, it would seem evident that substantial differences in removal rates in the several models are due to differences in treatment of the pertinent processes. Despite considerable differences in removal rates, the fraction of SO₂ that is removed by the several processes may be rather similar (e.g., the present model and that of *Lelieveld et al.* [1997]). Likewise despite the aqueous conversion in the present model being approximately twice as fast as in the model of *Roelofs et al.* [1998], that model indicates the fraction of SO₂ that is removed by aqueous conversion to be even greater than in the present model. Also presented in Table 10 is a comparison of the sulfate potential for several models, calculated as sulfate burden divided by the SO₂ emissions, which differs by approximately a factor of 2. Considerations such as these underscore the need to examine key physical diagnostics in

model comparisons, rather than simply assessing how well the models reproduce observed mixing ratios, as well as the potential utility of comparing such diagnostics with measurements from field studies. For detailed studies of the influence of aerosols on climate model representations, input data, evaluations with observations, and key physical diagnostics need to be examined in detail to try to elucidate the reasons for model-to-model differences and reduce them.

[58] In addition to the turnover times the main difference between *Benkovitz et al.* [1994] and the present study, the relative importance of the SO₂ sinks, can be explained by several factors. The meteorological conditions were different for the time periods of the two simulations. The meteorological data for the June–July 1986 study did not include cloud LWC information; the cloud model used calculated the LWC only for precipitating clouds, limiting the extent of the aqueous phase oxidation of SO₂. A limiting reagent formulation for the aqueous phase conversion by H₂O₂ was used in June–July 1986 study; this approach overestimates the oxidation of SO₂. In order to compare the relative conversion via the limiting reagent and via the full chemistry formulations a 1-hour simulation was performed using the limiting reagent formulation in Version 2 of GChM-O. In 94% of the locations where SO₂ was oxidized by H₂O₂, SO₂ was the limiting reagent; this fraction would be expected to vary for different seasons. The full kinetics mechanism always generated less sulfate; for the whole domain this mechanism generated only 44% of the sulfate generated by the limiting reagent mechanism.

[59] In the work presented here a large fraction of the discrepancies between the modeled and observed sulfate and SO₂ mixing ratios seems to be explained by the subgrid variability and measurement errors of these quantities. However, while overall the modeled sulfate concentration in precipitation was within a factor of 3 of the observed concentration, almost 75% of the concentrations were overestimated by the model, ~17% with $S_{m/o}$ values greater than 8. Values for the sulfate turnover times were close to those obtained from measurements of accumulation mode particles associated with the release of radionuclides. The relative values of key diagnostic quantities (turnover times, oxidation rates, etc.) by source region and source types can be understood in terms of the meteorological conditions prevalent during the simulation.

[60] A question that always needs to be asked in any modeling exercise is: are we getting the “right answers” for the “wrong reasons”? A possible reason for the closer agreement between modeled and observed sulfate and SO₂ MRs than for sulfate concentration in precipitation is that the SO₂ emissions and the oxidant concentrations were overestimated and the excess sulfate generated was removed by wet deposition, either because of deficiencies in the algorithms used for wet removal and the incorporation of aerosols into cloud water or because of overestimation of the precipitation values used by the model. Therefore several points of concern need to be addressed in the continued development and use of GChM-O. The wet removal algorithm used was a simplified representation that needs further testing and refinement. In addition, it does not account for either evaporation of falling precipitation in noncloudy layers or below-cloud scavenging of aerosols;

the importance of these processes needs to be examined, and if results indicate they are significant these processes must be represented in the algorithm. The algorithm used to represent the incorporation of aerosols into cloud water also needs further development and testing; for example, the values selected for f_{\max} , L_{mid} , and the limiting cloud liquid water fraction need to be further evaluated, although the overall rate of this process is likely much more sensitive to the frequency of encountering clouds than to the value of these parameters.

[61] The values of the oxidant MRs used were averages from a model that used meteorology from a GCM. As the GCM values did not reflect the actual meteorological conditions at the times and locations of the simulation, model simulations might be improved by use of more accurate representation of the oxidant MRs, which can be obtained if these MRs are calculated online in the CTM. Emissions for some regions and source types can vary significantly from year to year, especially for highly time-dependent sources such as volcanos and biogenic sources; more accurate emissions for the simulation period are needed, including more detailed breakdowns by season, release height, percent released as primary sulfate, and quantitative values of the uncertainties of these emissions.

[62] A two-week model spin-up time was used for the simulation presented here; time series plots of certain quantities such as sulfate yield indicated that a longer spin-up time would have been more appropriate for a simulation over the Northern Hemisphere domain used. Future simulations using this domain would seem to require a spin-up time of approximately one month.

6. Summary and Conclusions

[63] A Eulerian chemical transport model (CTM) for sulfate, the Global Chemistry Model driven by Observation-Derived Meteorology (GChM-O), has been developed to represent the sulfur cycle and to calculate distributions of sulfate, SO₂, DMS, and MSA with high spatial and temporal resolution, for specific times and locations, identified by source region, source type, and formation process. The model has been used to simulate the ACE-2 experimental period (June–July 1997) over the Northern Hemisphere from the equator to 81°N at 1° × 1° resolution and 27 vertical levels.

[64] Modeled MRs of sulfate and SO₂ and concentrations of sulfate in precipitation were evaluated using daily averaged sulfate and SO₂ MRs and event or weekly sulfate concentration in precipitation from observations by monitoring stations in North America, Europe, Taiwan, and stations in the Canary Islands and Korea. Concerns arise in these evaluations from lack of representativeness of the observational data sets. Many of the stations were under meteorological continental influence and were at least periodically impacted by proximate sources. In addition, for the majority of evaluations observed MRs for a model grid cell were based on a single monitoring station; thus cell-averaged model results were evaluated using point observations within the corresponding cell. This effect was examined and quantified using the median ratio characteristic spread (a measure of the variation of the ratios of observed quantities) of simultaneous observations which

provided the spatial variability within model grid cells and qualified the level of agreement that might be expected between modeled and observed quantities, especially for primary emitted species such as SO₂ or for sporadic phenomena such as precipitation. Median ratio characteristic spreads for simultaneous observations were 1.33 for sulfate, 2.32 for SO₂, and 1.36 for sulfate concentration in precipitation.

[65] The characteristic spreads between modeled and observed MRs for sulfate (5083 cases, median 1.85) and SO₂ (24155 cases, median 2.55) were comparable to, although somewhat greater than, those between observed MRs, indicating that departure between modeled and observed MRs was due in large part to the subgrid variation of the observed MRs. The median value of the characteristic spread between modeled and observed sulfate concentration in precipitation (2044 cases, median 2.82) was considerably larger than the spread between observations (127 cases, median 1.36), influenced in part by the proximate locations of stations within a grid cell and by differences between the precipitation used in the model and the actual precipitation at the monitoring stations.

[66] The differences between the modeled and observed MRs (a measure of model bias) for sulfate and SO₂ peaked at low values; the peaks included substantial contributions from a wide range of values of the observed MRs. The model almost equally overestimated and underestimated the sulfate observed MRs and overestimated somewhat over half of the SO₂ observed MRs. Over half of the modeled sulfate MRs were within a factor of 2 of the observed MRs, and over half of the modeled SO₂ MRs were within a factor of 3 of the observed MRs. Time series of the sulfate MRs demonstrated that model results closely track the magnitudes and temporal episodicity of the observed MRs.

[67] The major sink for sulfate and MSA was wet deposition (84–92% for sulfate, 87% for MSA); the two major sinks for SO₂ were aqueous-phase conversion to sulfate (50–69%) and dry deposition (6–29%), except for emissions from volcanic sources for which gas-phase conversion exceeded dry deposition. For sulfate and SO₂ turnover times differed substantially depending on source type, for sulfate from 4.3 to 9.0 days and for SO₂ from 0.7 to 2.2 days; turnover times were 3.9 days for MSA, and 1 day for DMS. Aerosol sulfate yields also differed substantially depending on source type, from 45 to 64%, and the MSA yield was 11%.

[68] Comparison of the results of this study with results from two previous studies that included analyses by source type or source region found discrepancies in the relative importance of sources on the resulting sulfate burden; in addition to differences in process representations in the models these discrepancies are influenced by the different meteorological conditions, emissions estimates, and length of the simulations presented (annual averages vs. a specific summer). Discrepancies of a factor of 2 or more remain in the removal rates, burden, lifetime, and contribution to sinks of both sulfate and SO₂ determined by the present study and those of other investigators. These differences directly affect the determination of the influence of aerosols on climate, indicating a need to examine the model representations, input data, and to evaluate with observations to try to elucidate and reduce these differences.

[69] In conclusion, the three-dimensional chemical transport model for sulfur described here is a powerful tool for examining sulfur mixing ratios and burdens by source region, source type, and formation process on a hemispheric to global scale, pertinent to the issues of radiative forcing by sulfate aerosol. Evaluation of sulfate and SO₂ MRs demonstrates that the model represents the observed sulfate and SO₂ MRs at fine temporal resolution with an accuracy comparable to the spatial variability and measurement error of the observed MRs. These analyses also demonstrate the importance of driving the model with meteorological quantities and other model input data representing as accurately as possible the conditions at the time when the observations were made.

Appendix A: Calculation of Mixed Layer Heights

[70] Time- and location-dependent mixed layer heights were obtained by a multistep approach based on calculated values of the equivalent potential temperature (θ_e), the saturation equivalent potential temperature (θ_{es}), the dew point (T_d), and the height (above ground) of the model vertical levels. For every model grid cell ($1^\circ \times 1^\circ$), referred to as a location, each successive step was applied only if the conditions of the previous steps were not met. (1) Convective cloud cases were identified when the meteorological data showed convective precipitation and a cloud base height less than 2 km. For these conditions air parcels rise through the mixed layer and then continue rising until they reach neutral buoyancy near the cloud top. A separate convective mixing algorithm was used within the cloud layer; therefore the mixing depth was set to the height of cloud base. (2) If no precipitation occurred in the grid cell, the thermodynamic profile was tested for convective instability. Profiles were defined as convectively unstable when θ_e at the surface exceeded θ_{es} at any height [Bohren and Albrecht, 1998]. A simplified parcel theory was used to approximate the depth of the mixing layer as the lowest level at which a parcel rising from the surface achieved neutral buoyancy (also called the level of free convection, LFC) under the assumption of a constant entrainment rate of $30\% \text{ km}^{-1}$ [Gregory, 2001]. When the LFC exceeded 4 km, the entrainment rate was decreased in steps of $1\% \text{ km}^{-1}$ until the height of the LFC was less than 4 km. (3) If no LFC below 4 km was found, convective boundary layer profiles were identified by testing for the presence of a subsidence inversion manifest in the decrease of humidity across the inversion. The mixing layer depth was defined as the height, less than or equal to X km, where the decrease in T_d between two successive model levels was 4 K or less; X was taken as 4 km for latitudes 0° – 15°N , as 3 km for latitudes 15° – 60°N [Albrecht et al., 1995] and as 2 km for latitudes greater than 60°N [Uttal et al., 2002]. (4) For locations that did not satisfy any of these criteria the vertical profile was considered to be stable (i.e., parcels displaced vertically tend to return to their original level), and the mixed layer height was set to the height of the first model level above the surface.

Appendix B: Calculation of DMS Emissions From the Ocean

[71] Time- and location-dependent dimethylsulfide (DMS) emissions from the ocean were estimated using

sea surface DMS concentrations and the wind speed transfer function of *Liss and Merlivat* [1986]. The data source for the sea surface DMS concentrations was the global data set compiled by *Kettle et al.* [1999], which includes over 15,000 point measurements throughout the world oceans taken between March 1972 and October 1997. DMS concentrations in middle and high latitudes have a strong seasonal dependency [*Kettle et al.*, 1999]; the timing of this seasonality depends on a combination of physical, chemical and biological processes. The DMS measurements in the *Kettle et al.* database for June and July were used for the Atlantic and Pacific Oceans; the selected data included only open ocean measurements as coastal and estuarine DMS concentrations are generally higher than open ocean concentrations and representative of only small areas around the measurement location. A water depth of 100 m was used to differentiate between open ocean and coastal measurements (C. Wirick, Brookhaven National Laboratory, personal communication, 1999). The selected data set included 646 measurements in the Atlantic Ocean and 191 measurements in the Pacific Ocean.

[72] The surface DMS concentrations chosen were used to create a $1^\circ \times 1^\circ$ resolution grid using a geostatistical methodology known as kriging [*Isaaks and Srivastava*, 1989]. Kriging generates an estimated surface from a scattered set of points based on regionalized variable theory that assumes that the same pattern of variation can be observed at all locations on the surface. Kriging is an excellent linear unbiased estimator because (1) low weights are assigned to distant samples and higher weights are assigned to proximate samples and (2) the relative position of the samples to each other as well as the area being examined are taken into account. The spatial variation is quantified by a semivariogram; the semivariogram is modeled by fitting a theoretical function to the sample semivariogram. The geographic information system software Arc/Info used assumes that the variation in the values is free from any structural component. The surface estimator can be calculated using spherical, circular, exponential, Gaussian and linear methods. Kriging uses the mathematical function selected to fit a line or curve to the semivariance data in the semivariogram. For each ocean, the DMS concentrations were krigged using each of the five methods indicated above for several cell resolutions. The optimum cell size and method were selected to maintain the regional features in the DMS data set but to eliminate small hot spots.

[73] Within the ACE-2 study area the ACE-2 surface DMS data were used, as these measurements best reflected the conditions for June–July 1997 [*Bates et al.*, 2000]. Measurements showed that the sea surface temperature and salinity in the experimental region varied linearly with latitude ranging from 23°C, 36.8 PSU, in the south (29°N) to 18°C, 35.8 PSU, in the north (41°N). Surface seawater DMS concentrations during ACE-2 were relatively

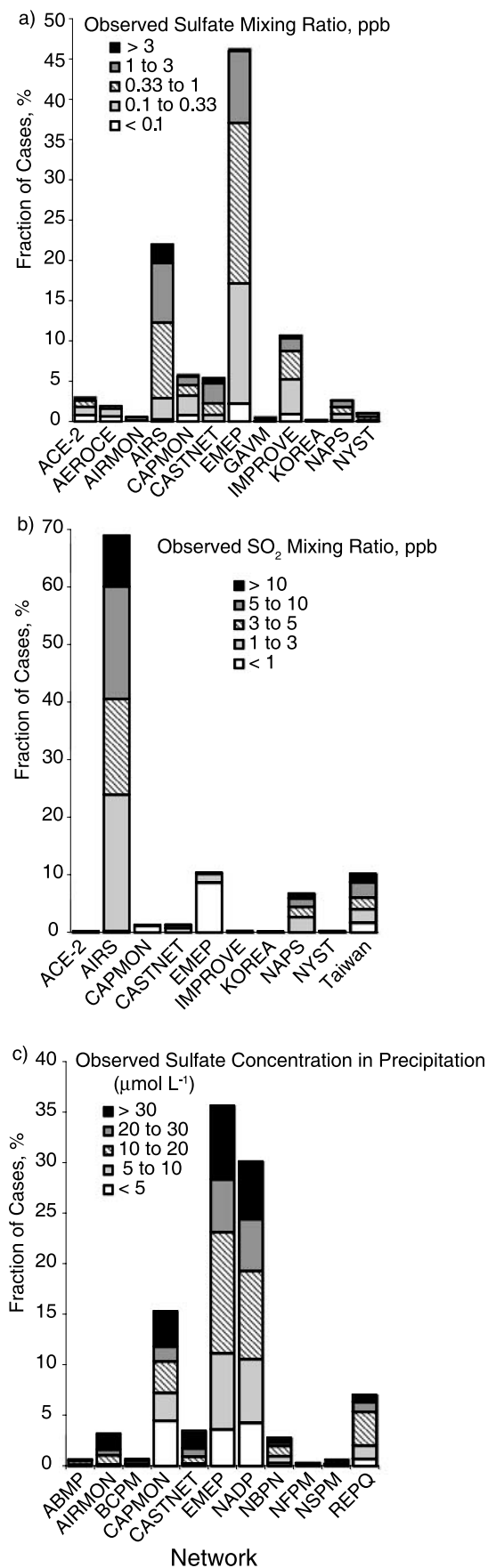


Figure C1. Histogram of the distribution of observations among networks: (a) sulfate mixing ratios, (b) SO₂ mixing ratios, and (c) sulfate concentration in precipitation. Shading denotes fraction of observations for which mixing ratios or concentrations were within the individual ranges.

uniform during the first three weeks of the campaign averaging 1.3 ± 0.2 nM for distances greater than 40 km from the Portugal coast, which is outside the upwelling waters identified on the basis of temperature and salinity. During the final week, concentrations in the offshore region west of Portugal began to increase, reaching 2.7 nM by the end of the campaign [Bates *et al.*, 2000]. The field measurements were krigged over the experimental area and used to replace the Kettle *et al.* [1999] krigged values.

[74] Sea surface temperatures from the Kettle *et al.* [1999] database were gridded using the same procedure. The gridded temperature and DMS sea surface concentrations were combined with ECMWF wind speeds at 6-hour intervals to calculate DMS emission fluxes using the Liss and Merlivat [1986] wind speed transfer velocity relationship.

Appendix C: Summary of Observations Used in Model Evaluation

[75] The sulfate observational data set consisted of 6067 measurements at 481 stations in 12 different networks; sampling duration times varied from 1 to 7 days, with over 90% of the sampling being 1 day or less. Almost 50% of the measurements were from the EMEP network (Figure C1a), $\sim 23\%$ were from the AIRS network, with the rest of the networks each contributing 10% or less. After averaging concurrent measurements at each location to obtain the observed MRs, there were 5083 cases available at 320 locations. The majority of the observed MRs ($\sim 63\%$) were less than or equal to 0.66 ppb, with $\sim 3\%$ greater than 3 ppb. There were concurrent measurements in $\sim 6\%$ of the cases; all cases were located in North America except for those at the ACE-2 stations at Tenerife, Canary Islands. The multiple observations set exhibited somewhat greater MRs than the data set as a whole (Figure C2a), probably a reflection of greater density of measurements in locations with larger sulfate MRs in support of air quality assessment or compliance.

[76] The SO_2 observational data set included 24155 measurements from 893 stations in 10 different networks; sampling duration times (or reported averaging times in the case of real-time instruments) varied from 1 hour to 7 days, with over 98% of the sampling being 24 hours or less. The measurements were averaged to 24 hours when needed; little is gained in evaluating 6-hour modeled MRs with 6-hour averaged observed MRs as versus the 24-hour averages [Benkovitz and Schwartz, 1997]. Almost 70% of the measurements were from the AIRS network (Figure C1b), with the rest of the networks each contributing $\sim 10\%$ or less. After averaging concurrent measurements in each location to obtain the observed MRs there were 12624 cases available at 414 locations. The majority of the observed MRs ($\sim 55\%$) were less than or equal to 3 ppb, with $\sim 7\%$ greater than 10 ppb. There were concurrent measurements in $\sim 28\%$ of the cases; all are located in North America except for some cases located in Taiwan. For the multiple

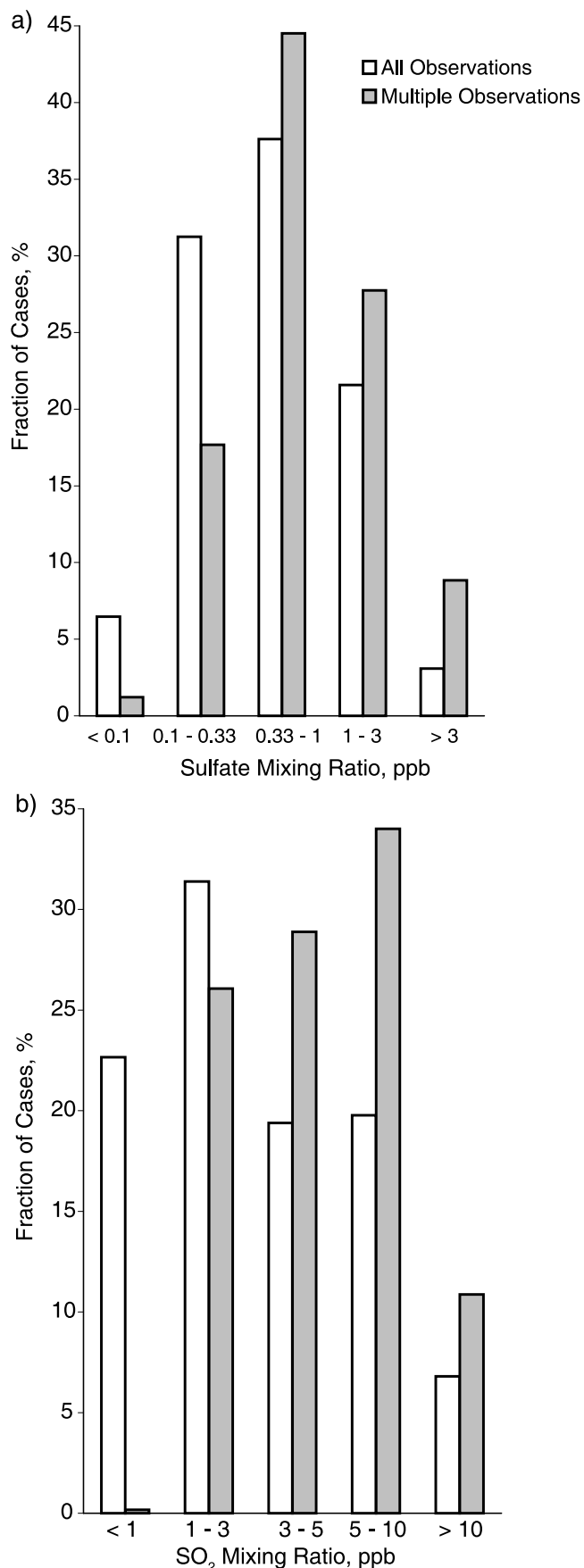


Figure C2. Histograms of the distribution of the observed mixing ratios for the data set containing multiple observations within a location and of the whole data set: (a) sulfate and (b) SO_2 .

observations set (Figure C2b), very few MRs were less than 1 ppb, with the majority (~63%) in the 3 to 10 ppb range; in contrast for the entire data set almost 25% of the MRs were less than 1 ppb, with the majority (~54%) less than or equal to 3 ppb.

[77] There were a total of 521 evaluation locations for sulfate or SO₂; ~20% had sulfate observations only, ~39% had SO₂ observations only and ~41% had both sulfate and SO₂ observations.

[78] The concentration of sulfate in precipitation was measured by 11 networks with 369 stations; observed concentrations corrected for sea salt sulfate were used in these evaluations. The networks monitored 2366 events, of which 2187 (~92%) were captured in the model (i.e., the meteorological data indicated rain within the time period for which precipitation was collected), from 100% for more than half of the networks to 84% for EMEP. The EMEP network contributed the highest number of events, (Figure C1c), followed by NADP and CAPMoN, with the rest of the networks contributing substantially less. After averaging concurrent measurements in each location to obtain the observed concentrations there were 2044 cases available for evaluation at 316 locations. The majority of the observed concentrations (~51%) were less than or equal to 15 μmol L⁻¹, with ~13% greater than 40 μmol L⁻¹. There were concurrent measurements in ~6% of the cases.

[79] **Acknowledgments.** Research by BNL investigators was performed under the auspices of the U.S. Department of Energy under contract DE-AC02-98CH10886. The meteorological data used to drive the model were obtained from the European Centre for Medium-Range Weather Forecasts (ECMWF), Reading, UK. As listed in Table 5, some of the sulfate and wet deposition data used in this work were provided by the Canadian National Atmospheric Chemistry (NatChem) Database and its data-contributing agencies and organizations. We thank the principal investigators listed in Table 3 for supplying the measurements of volcanic SO₂ emissions. We thank M. Altaf Mubarakhi for his help in this project.

References

- Albrecht, B. A., M. P. Jensen, and W. J. Syrett (1995), Marine boundary layer structure and fractional cloudiness, *J. Geophys. Res.*, *100*(D7), 14,209–14,222.
- Andres, R. J., and S. D. Kasgnoc (1998), A time-averaged inventory of subaerial volcanic sulfur emissions, *J. Geophys. Res.*, *103*(D19), 25,251–25,261.
- Barrie, L. A., et al. (2001), A Comparison of Large Scale Atmospheric Sulphate Aerosol Models (COSAM): Overview and highlights, *Tellus, Ser. B*, *53*, 615–645.
- Barth, M. C., P. J. Rasch, J. T. Kiehl, C. M. Benkovitz, and S. E. Schwartz (2000), Sulfur chemistry in the National Center for Atmospheric Research Community Climate Model: Description, evaluation, features and sensitivity to aqueous chemistry, *J. Geophys. Res.*, *105*(D1), 1387–1415.
- Bates, T. S., B. K. Lamb, A. Guenther, J. Dignon, and R. E. Stoiber (1992), Sulfur emissions to the atmosphere from natural sources, *J. Atmos. Chem.*, *14*, 315–337.
- Bates, T. S., P. K. Quinn, D. S. Covert, D. J. Coffman, J. E. Johnson, and A. Wiedensohler (2000), Aerosol physical properties and processes in the lower marine boundary layer: A comparison of shipboard sub-micron data from ACE-1 and ACE-2, *Tellus, Ser. B*, *52*, 258–272.
- Benkovitz, C. M., and S. E. Schwartz (1997), Evaluation of modeled sulfate and SO₂ over North America and Europe for four seasonal months in 1986–87, *J. Geophys. Res.*, *102*(D21), 25,305–25,338.
- Benkovitz, C. M., C. M. Berkowitz, R. C. Easter, S. Nemesure, R. Wagener, and S. E. Schwartz (1994), Sulfate over the North Atlantic and adjacent continental regions: Evaluation for October and November, 1986 using a three-dimensional model driven by observation-derived meteorology, *J. Geophys. Res.*, *99*(D10), 20,725–20,756.
- Benkovitz, C. M., J. J. M. Berdowski, M. A. Mubarakhi, and J. G. J. Olivier (1996), Global anthropogenic sulfur emissions for 1985 and 1990, in *Assessing Historical Global Sulfur Emission Patterns for the Period 1850–1990*, edited by A. S. Lefohn, J. D. Husar, and R. B. Husar, pp. A1–A45, U.S. Dep. of Energy, Washington, D. C.
- Benkovitz, C. M., S. E. Schwartz, and B.-G. Kim (2003), Evaluation of a chemical transport model for sulfate using ACE-2 observations and attribution of sulfate mixing ratios to source regions and formation processes, *Geophys. Res. Lett.*, *30*(12), 1641, doi:10.1029/2003GL016942.
- Benkovitz, C. M., H. Akimoto, J. J. Corbett, J. D. Mobley, J. G. J. Olivier, J. A. van Aardenne, and V. Vestreng (2004), Compilation of regional to global inventories of anthropogenic emissions, in *Emissions of Atmospheric Trace Compounds*, edited by C. Granier, P. Artaxo, and C. E. Reeves, pp. 19–78, Kluwer Acad., Norwell, Mass.
- Bohren, C. F., and B. A. Albrecht (1998), *Atmospheric Thermodynamics*, 402 pp., Oxford Univ. Press, New York.
- Bott, A. (1989), A positive definite advection scheme obtained by nonlinear renormalization of the advective fluxes, *Mon. Weather Rev.*, *117*, 1006–1015.
- Brasseur, G. P., and S. Madronich (1992), Chemistry-transport models, in *Climate System Modeling*, edited by K. E. Trenberth, pp. 491–518, Cambridge Univ. Press, New York.
- Brasseur, G., D. Hauglustaine, S. Walters, P. Rasch, J. Müller, G. Granier, and X. X. Tie (1998), MOZART: A global chemical transport model for ozone and related chemical tracers: 1. Model description, *J. Geophys. Res.*, *103*(D21), 28,265–28,289.
- Cambay, R. S., P. A. Cawse, J. A. Garland, J. A. B. Gibson, P. Johnson, G. N. J. Lewis, D. Newton, L. Salmon, and B. O. Wade (1987), Observations on radioactivity from the Chernobyl accident, *Nucl. Energy*, *26*, 77–101.
- Chamberlain, A. C. (1991), *Radioactive Aerosols*, Cambridge Univ. Press, New York.
- Charlson, R., S. E. Schwartz, J. M. Hales, R. D. Cess, J. J. A. Coakley, J. E. Hansen, and D. J. Hoffman (1992), Climate forcing by anthropogenic aerosols, *Science*, *255*, 423–430.
- Cherubini, T., A. Ghelli, and F. Lalaurette (2001), Verification of precipitation forecasts over the alpine region using a high density observing network, *ECMWF Tech. Memo. 340*, 18 pp., Eur. Cent. for Medium-Range Weather Forecasts, Reading, UK.
- Chin, M., R. B. Rood, S.-J. Lin, J.-F. Müller, and A. M. Thompson (2000a), Atmospheric sulfur cycle simulated in the global model GOCART: Model description and global properties, *J. Geophys. Res.*, *105*(D20), 24,671–24,687.
- Chin, M., D. L. Savoie, B. J. Huebert, A. R. Bandy, D. C. Thornton, T. S. Bates, P. K. Quinn, E. S. Saltzman, and W. J. D. Bryun (2000b), Atmospheric sulfur cycle simulated in the global model GOCART: Comparison with field observations and regional budgets, *J. Geophys. Res.*, *105*(D20), 24,689–24,712.
- Cowling, E. B. (1982), Acid precipitation in historical perspective, *Environ. Sci. Technol.*, *16*, 110A–123A.
- Daum, P. H., S. E. Schwartz, and L. Newman (1984), Acidic and related constituents in liquid water stratiform clouds, *J. Geophys. Res.*, *89*(D1), 1447–1458.
- DeMore, W. B., S. P. Sander, D. M. Golden, R. F. Hampson, M. J. Kurylo, C. J. Howard, A. R. Ravishankara, C. E. Kolb, and M. J. Molina (1997), Chemical kinetics and photochemical data for use in stratospheric modeling: Evaluation 12, *JPL Publ. 97-4*, 266 pp.
- Easter, R. C. (1993), Two modified versions of Bott's positive definite numerical advection scheme, *Mon. Weather Rev.*, *121*, 297–304.
- Easter, R. C., and D. J. Luecken (1988), A simulation of sulfur wet deposition and its dependence on the inflow of sulfur species to storms, *Atmos. Environ.*, *22*, 2715–2739.
- Elias, T., A. J. Sutton, J. B. Stokes, and T. J. Casadevall (1998), Sulfur dioxide emission rates of Kilauea Volcano, Hawaii, 1979–1997, pp. 41, Hawaii Volcano Obs., U.S. Geol. Surv., Hawaii Volcanoes Natl. Park.
- Erickson, R. E., L. M. Yates, R. L. Clark, and D. MacEwen (1977), The reaction of sulfur dioxide with ozone in water and its possible atmospheric significance, *Atmos. Environ.*, *11*, 813–817.
- European Centre for Medium-Range Weather Forecasts (ECMWF) (2003), IFS documentation cycle CY25r1, parts I–VII, Reading, England.
- Feichter, J., U. Lohmann, and I. Schult (1997), The atmospheric sulfur cycle in ECHAM-4 and its impact on the shortwave radiation, *Clim. Dyn.*, *13*, 235–246.
- Goldberg, R. N., and V. B. Parker (1985), Thermodynamics of solution of SO₂(g) in water and of aqueous sulfur dioxide solutions, *J. Res. Natl. Bur. Stand. U.S.*, *90*(5), 341–358.
- Graf, H.-F., J. Feichter, and B. Langmann (1997), Volcanic sulfur emissions: Estimates of source strength and its contribution to the global sulfate distribution, *J. Geophys. Res.*, *102*(D9), 10,727–10,738.
- Gregory, D. (2001), Estimation of entrainment rate in simple models of convective clouds, *Q. J. R. Meteorol. Soc.*, *127*, 53–72.
- Guenther, A., et al. (1995), A global model of natural volatile organic compound emissions, *J. Geophys. Res.*, *100*(D5), 8873–8892.

- Haywood, J. M., and K. P. Shine (1995), The effect of anthropogenic sulfate and soot aerosol on the clear sky planetary radiation budget, *Geophys. Res. Lett.*, **22**, 603–606.
- Heald, C. L., D. J. Jacob, P. I. Palmer, M. J. Evans, G. W. Sachse, H. B. Singh, and D. R. Blake (2003), Biomass burning emission inventory with daily resolution: Application to aircraft observations of Asian outflow, *J. Geophys. Res.*, **108**(D21), 8811, doi:10.1029/2002JD003082.
- Hoigné, J., H. Bader, W. R. Haag, and J. Staehelin (1985), Rate constants of reactions of ozone with organic and inorganic compounds in water: III, *Water Res.*, **19**(8), 993–1004.
- Horowitz, L. W., S. Walters, D. Mauzerall, L. Emmons, P. Rasch, C. Granier, X. Tie, J. F. Lamarque, M. Schultz, and G. Brasseur (2003), A global simulation of tropospheric ozone and related tracers: Description and evaluation of MOZART, version 2, *J. Geophys. Res.*, **108**(D24), 4784, doi:10.1029/2002JD002853.
- Isaaks, E. H., and R. M. Srivastava (1989), *An Introduction to Applied Geostatistics*, Oxford Univ. Press, New York.
- Jaffe, D., I. McKendry, T. Anderson, and H. Price (2003), Six 'new' episodes of trans-pacific transport of air pollutants, *Atmos. Environ.*, **37**, 391–404.
- Jung, T., and A. Tompkins (2003), Systematic errors in the ECMWF forecasting system, *ECMWF Tech. Memo.* **422**, 72 pp., Reading, UK.
- Kettle, A. J., and M. O. Andreae (2000), Flux of dimethylsulfide from the oceans: A comparison of updated data and flux models, *J. Geophys. Res.*, **105**(D22), 26,793–26,808.
- Kettle, A. J., et al. (1999), A global database of sea surface dimethyl sulfide (DMS) measurements and a procedure to predict sea surface DMS as a function of latitude, longitude, and month, *Global Biogeochem. Cycles*, **13**, 399–444.
- Ko, M. K., and N.-D. Sze (1991), Impact on stratospheric ozone from emissions of CFCs and substitutes: A two-dimensional model assessment, in *Atmospheric Chemistry Models and Predictions for Climate and Air Quality*, edited by C. S. Sloane and T. W. Tesche, pp. 9–24, Lewis, Chelsea, Mich.
- Koch, D., D. Jacob, I. Tegen, D. Rind, and M. Chin (1999), Tropospheric sulfur simulation and sulfate direct radiative forcing in the Goddard Institute for Space Studies general circulation model, *J. Geophys. Res.*, **104**(D19), 23,799–23,822.
- Koch, D., J. Park, and A. D. Genio (2003), Clouds and sulfate are anticorrelated: A new diagnostic for global sulfur models, *J. Geophys. Res.*, **108**(D24), 4781, doi:10.1029/2003JD003621.
- Kuylenstierna, J. C. I., H. Rodhe, S. Cinderby, and K. K. Hicks (2001), Acidification in developing countries: Ecosystem sensitivity and the critical load approach on a global scale, *Ambio*, **30**, 20–28.
- Lalaurette, F., L. Ferranti, A. Ghelli, and G. van der Grijn (2003), Verification statistics and evaluations of ECMWF forecasts in 2002–2003, *ECMWF Tech. Memo.* **432**, 48 pp., Reading, UK.
- Langner, J., and H. Rodhe (1991), A global three-dimensional model of the tropospheric sulfur cycle, *J. Atmos. Chem.*, **13**, 225–263.
- Leaitch, W. R., J. W. Strapp, H. A. Wiebe, and G. A. Isaac (1983), Measurements of scavenging and transformation of aerosol inside cumulus, in *Precipitation Scavenging, Dry Deposition and Resuspension*, edited by R. G. S. H. R. Pruppacher and W. G. N. Slinn, pp. 53–69, Elsevier Sci., New York.
- Lelieveld, J., G.-J. Roelofs, L. Ganzeveld, J. Feichter, and H. Rodhe (1997), Terrestrial sources and distribution of atmospheric sulfur, *Philos. Trans. R. Soc. London, Ser. B*, **352**, 149–158.
- Liss, P. S., and L. Merlivat (1986), Air-sea gas exchange rates: Introduction and synthesis, in *The Rate of Air-Sea Exchange in Geochemical Cycling*, edited by P. Buat-Menard, pp. 113–127, D. Reidel, Norwell, Mass.
- Lohmann, U., et al. (2001), Vertical distributions of sulfur species simulated by large scale atmospheric models in COSAM: Comparison with observations, *Tellus, Ser. B*, **53**, 646–672.
- Louis, J.-F. (1979), A parameteric model of vertical eddy fluxes in the atmosphere, *Boundary Layer Meteorol.*, **17**, 187–202.
- Mather, T. A., D. M. Pyle, and C. Oppenheimer (2003), Tropospheric volcanic aerosol, in *Volcanism and the Earth's Atmosphere*, *Geophys. Monogr. Ser.*, vol. 139, edited by A. Robock and C. Oppenheimer, pp. 189–212, AGU, Washington, D. C.
- McNair, L. A., R. A. Harley, and A. G. Russell (1996), Spatial inhomogeneity in pollutant concentrations, and their implications for air quality model evaluation, *Atmos. Environ.*, **30**, 4291–4301.
- Mullen, S. L., and R. Buizza (2001), Quantitative precipitation forecasts over the United States by the ECMWF Ensemble Prediction System, *Mon. Weather Rev.*, **129**(4), 638–663.
- Müller, J. F. (1992), Geographical distribution and seasonal variation of surface emissions and deposition velocities of atmospheric trace gases, *J. Geophys. Res.*, **97**, 3787–3804.
- Müller, J.-F., and G. Brasseur (1995), IMAGES: A three-dimensional chemical transport model of the global troposphere, *J. Geophys. Res.*, **100**(D8), 16,445–16,490.
- National Research Council Panel on Aerosol Radiative Forcing and Climate (1996), *A Plan for a Research Program on Aerosol Radiative Forcing and Climate Change*, edited by J. Seinfeld, Natl. Acad. Press, Washington, D. C.
- Olivier, J. G. J., and J. J. M. Berdowski (2001), Global emissions sources and sinks, in *The Climate System*, edited by J. Berdowski, R. Guicherit, and B. J. Heij, pp. 33–78, Swets and Zeitlinger, Lisse, Netherlands.
- Olivier, J. G. J., A. F. Bouwman, C. W. M. van der Maas, J. J. M. Berdowski, C. Veldt, J. P. J. Bloos, A. J. H. Visschekijk, P. Y. J. Zandveld, and J. L. Haverlag (1996), Description of EDGAR version 2: A set of global emissions inventories of greenhouse gases and ozone-depleting substances for all anthropogenic and most natural sources on a per country basis and on $1^\circ \times 1^\circ$ grid, Natl. Inst. of Public Health and the Environ., Bilthoven, Netherlands.
- Olivier, J. G. J., J. A. H. W. Peters, J. Bakker, J. J. M. Berdowski, A. J. H. Visschedijk, and J. P. J. Bloos (2002), *Applications of EDGAR: Emissions Database for Global Atmospheric Research*, 151 pp., Natl. Inst. of Public Health and the Environ., Bilthoven, Netherlands.
- Overton, J. H. (1985), Validation of the Hoffmann and Edwards' S (IV)-H₂O₂ mechanism, *Atmos. Environ.*, **19**, 687–690.
- Pasquill, F. (1976), The dispersion of material in the atmospheric boundary layer: The basis for generalization, in *Lectures on Air Pollution and Environmental Impact Analyses*, edited by D. A. Haugen, pp. 1–34, Am. Meteorol. Soc., Boston, Mass.
- Penner, J., et al. (2001), Aerosols: Their direct and indirect effects, in *Climate Change 2001: The Scientific Basis*, edited by J. T. Houghton et al., pp. 289–348, Cambridge Univ. Press, New York.
- Pickering, K. E., Y. Wang, W.-K. Tao, C. Price, and J.-F. Muller (1998), Vertical distributions of lightning NO_x for use in regional and global chemical transport models, *J. Geophys. Res.*, **103**(D23), 31,203–31,216.
- Prasad, V., Y. Kant, P. K. Gupta, C. Elvidge, and K. V. S. Badarinarath (2002), Biomass burning and related trace gas emissions from tropical dry deciduous forests of India: A study using DMSP-OLS data and ground-based measurements, *Int. J. Remote Sens.*, **23**(14), 2837–2851.
- Price, C., J. Penner, and M. Prather (1997), NO_x from lightning: 1. Global distribution based on lightning physics, *J. Geophys. Res.*, **102**(D5), 5929–5941.
- Prospero, J. M. (1999), Long-term measurements of the transport of African mineral dust to the southeastern United States: Implications for regional air quality, *J. Geophys. Res.*, **104**(D13), 15,917–15,927.
- Raes, F., T. Bates, F. McGovern, and M. V. Liedekerke (2000), The 2nd Aerosol Characterization Experiment (ACE-2): General overview and main results, *Tellus, Ser. B*, **52**, 111–125.
- Ramaswamy, V., O. Boucher, J. Haigh, D. Hauglustaine, J. Haywood, G. Myhre, T. Nakajima, G. Y. Shi, and S. Solomon (2001), Radiative forcing of climate change, in *Climate Change 2001: The Scientific Basis*, edited by J. T. Houghton et al., pp. 349–416, Cambridge Univ. Press, New York.
- Rasch, P. J., M. C. Barth, J. T. Kiehl, S. E. Schwartz, and C. M. Benkovitz (2000a), A description of the global sulfur cycle and its controlling processes in NCAR CCM3, *J. Geophys. Res.*, **105**(D1), 1367–1385.
- Rasch, P. J., et al. (2000b), A comparison of scavenging and deposition processes in global models: Results from the WCRP Cambridge Workshop of 1995, *Tellus, Ser. B*, **52**, 1025–1056.
- Ro, C. U., and R. J. Vet (2002), Analyzed data fields from the National Atmospheric Chemistry Database (NATChem) and Analysis Facility, Air Qual. Res. Branch, Meteorol. Serv. of Can., Environ. Can., Toronto, Ont.
- Roelofs, G.-J., and J. Lelieveld (1995), Distribution and budget of O₃ in the troposphere calculated with a chemistry general circulation model, *J. Geophys. Res.*, **100**(D10), 20,983–20,998.
- Roelofs, G.-J., J. Lelieveld, and L. Ganzeveld (1998), Simulation of global sulfate distribution and the influence on effective cloud drop radii with a coupled photochemistry-sulfur cycle model, *Tellus, Ser. B*, **50**, 224–242.
- Roelofs, G.-J., et al. (2001), Analysis of regional budgets of sulfur species modeled for the COSAM exercise, *Tellus, Ser. B*, **53**, 673–694.
- Rotstajn, L. D., and U. Lohmann (2002), Simulation of the tropospheric sulfur cycle in a global model with a physically based cloud scheme, *J. Geophys. Res.*, **107**(D21), 4592, doi:10.1029/2002JD002128.
- Schwartz, S. E. (1988), Mass-transport limitation to the rate of in-cloud oxidation of SO₂: Re-examination in the light of new data, *Atmos. Environ.*, **22**, 2491–2499.
- Sheih, C. M., M. L. Wesely, and C. J. Walcek (1986), A dry deposition module for regional acid deposition, U.S. Environ. Prot. Agency, Research Triangle Park, N. C.
- Spiro, P. A., D. J. Jacob, and J. A. Logan (1992), Global inventory of sulfur emissions with a $1^\circ \times 1^\circ$ resolution, *J. Geophys. Res.*, **97**(D5), 6023–6036.
- Stockwell, W. R. (1995), ON the HO₂ + HO₂ reaction: Its misapplication in atmospheric chemistry models, *J. Geophys. Res.*, **100**(D6), 1695–1698.

- Streets, D. G., N. Y. Tsai, H. Akimoto, and K. Oka (2000), Sulfur dioxide emissions in Asia in the period 1985–1997, *Atmos. Environ.*, *34*, 4413–4424.
- Streets, D. G., N. Y. Tsai, H. Akimoto, and K. Oka (2001), Trends in emissions of acidifying species in Asia, 1985–1997, *Water Air Soil Pollut.*, *130*, 187–192.
- Talbot, R. W., R. C. Harriss, E. V. Browell, G. L. Gregory, E. I. Sebacher, and S. M. Beck (1986), Distribution and geochemistry of aerosols in the tropical North Atlantic troposphere: Relationship to Saharan dust, *J. Geophys. Res.*, *91*, 5173–5182.
- ten Brink, H. M., S. E. Schwartz, and P. H. Daum (1987), Efficient scavenging of aerosol sulfate by liquid-water clouds, *Atmos. Environ.*, *21*, 2035–2052.
- U.S. Environmental Protection Agency (2000), National air pollutant emission trends: 1900–1998, *EPA 454/R-00-002*, Research Triangle Park, N. C.
- U.S. Environmental Protection Agency (2001), National air quality and emissions trends report: 1999, *EPA 454/R-01-004*, 237 pp., Off. of Air Qual. Plann. and Stand., Research Triangle Park, N. C.
- Uttal, T., et al. (2002), Surface heat budget of the Arctic Ocean, *Bull. Am. Meteorol. Soc.*, *83*(2), 255–276.
- Vedal, S. (1997), Ambient particles and health: Lines that divide, *J. Air Waste Manage. Assoc.*, *47*(5), 551–558.
- Vestreng, V., and H. Klein (2002), Emission data reported to UNECE/EMEP: Quality assurance and trends analysis, 101 pp., Meteorol. Syn. Cent.-West, Oslo.
- Walcek, C. J., and G. R. Taylor (1986), A theoretical method for computing vertical distributions of acidity and sulfate production within cumulus clouds, *J. Atmos. Sci.*, *43*, 339–355.
- Wesely, M. (1989), Parameterization of surface resistances to gaseous dry deposition in regional-scale numerical models, *Atmos. Environ.*, *23*, 1293–1304.
- Wooster, M. J., and N. Strub (2002), Study of the 1997 Borneo fires: Quantitative analysis using global area coverage (GAC) satellite data, *Global Biogeochem. Cycles*, *16*(1), 1009, doi:10.1029/2000GB001357.
- Wotawa, G., and M. Trainer (2000), The influence of Canadian forest fires on pollutant concentrations in the United States, *Science*, *288*, 324–328.
- Yienger, J. J., and H. Levy (1995), Empirical model of global soil-biogenic NO_x emissions, *J. Geophys. Res.*, *100*(D6), 11,447–11,464.
- Yin, F., D. Grosjean, and J. H. Seinfeld (1990a), Photooxidation of dimethyl sulfide and dimethyl disulfide. I: Mechanism development, *J. Atmos. Chem.*, *11*, 309–364.
- Yin, F., D. Grosjean, R. C. Flagan, and J. H. Seinfeld (1990b), Photooxidation of dimethyl sulfide and dimethyl disulfide. II: Mechanism evaluation, *J. Atmos. Chem.*, *11*, 365–399.

T. S. Bates, Pacific Marine Environmental Laboratory, Seattle, WA 98115, USA.

C. M. Benkovitz, M. A. Miller, and S. E. Schwartz, Brookhaven National Laboratory, Upton, NY 11973, USA. (cmb@bnl.gov)

R. C. Easter, Pacific Northwest National Laboratory, Richland, WA 99352, USA.

M. P. Jensen, Department of Applied Physics and Applied Mathematics, Columbia University, New York, NY 10027, USA.

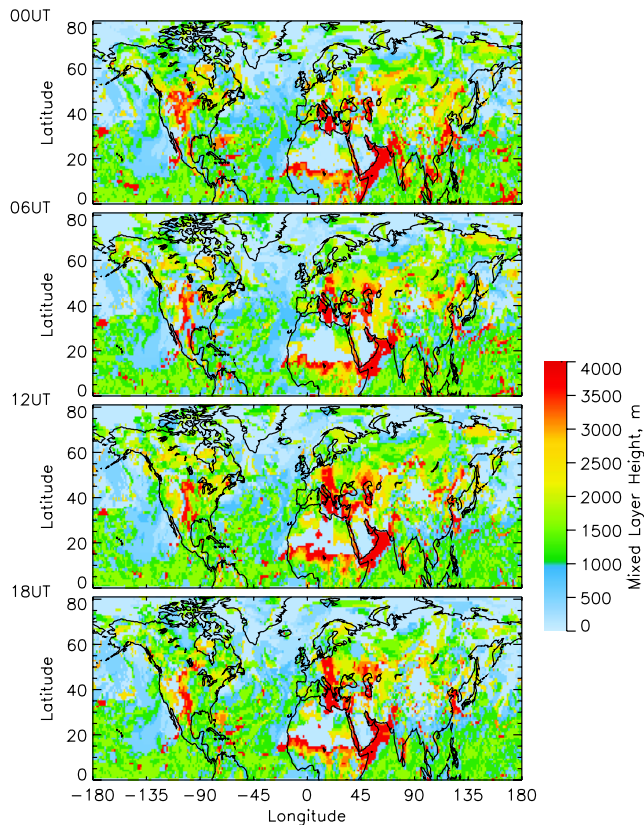


Figure 2. Heights of the mixed layer for 29 June 1997. Note the general increase in height over the oceans from the poles to the tropics, the relatively lower depths over regions of ocean upwelling such as off the coast of California, and the clear diurnal cycle particularly over land (for example, the European continent shows relatively lower height over the entire region at 0000 UT compared to 1200 UT).

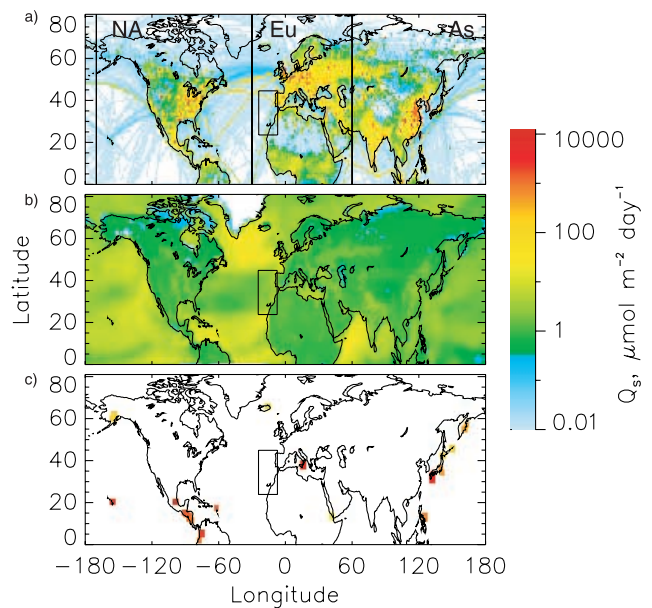


Figure 4. Sulfur emissions for the simulation period: (a) anthropogenic sources, (b) average biogenic sources, and (c) average volcanic sources. All panels use the scale shown. Volcanic emissions were divided by the area of the model grid cell where the volcano is located. The vertical lines in Figure 4a delimit the anthropogenic source regions distinguished in the model, North America (NA), Europe (Eu), and Asia (As). The rectangle delimits the ACE-2 experimental area (25°–8°W longitude; 23°–44°N latitude).

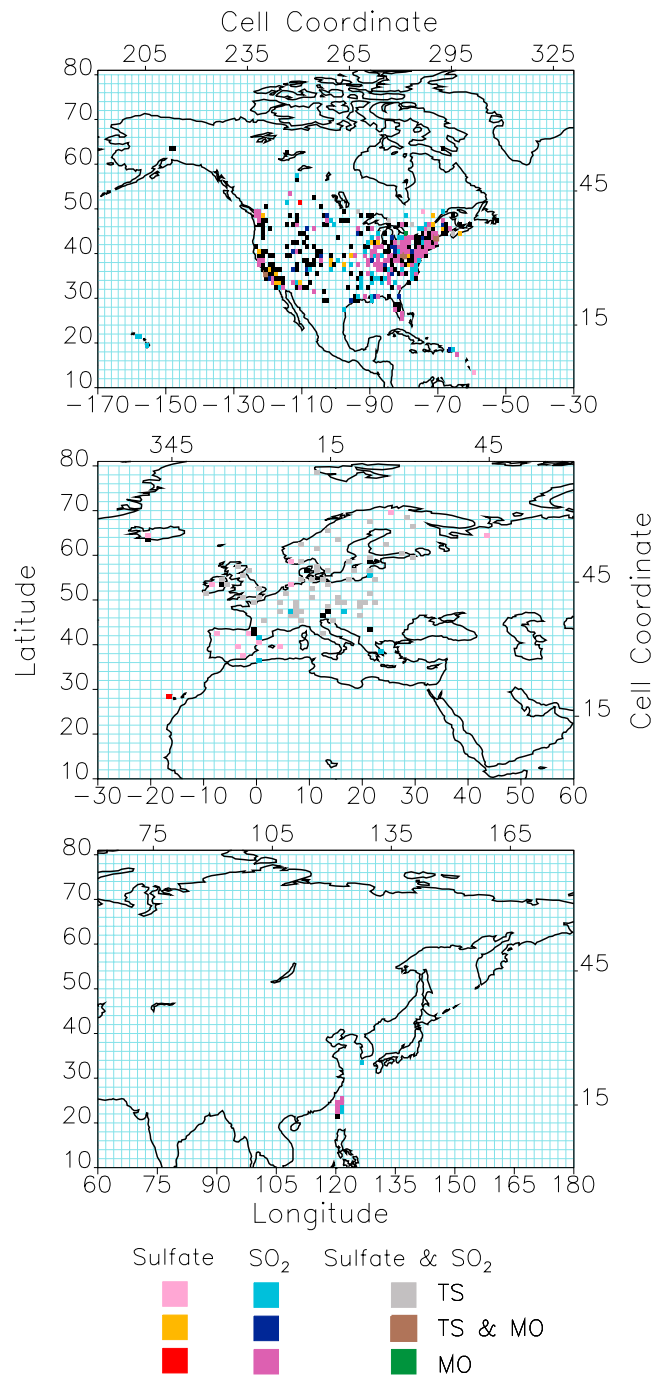


Figure 5. Map of the evaluation locations for sulfate and SO₂. TS denotes locations for which time series data were available, and MO denotes locations at which there were multiple observations.



Figure 6. Time series of the modeled and observed sulfate mixing ratios at the 90 locations that had at least 28 observations for the period 17 June to 24 July 1997. The three numbers, i, j, k , at the top right of each panel represent the three-dimensional model coordinates of the location. Model domain is numbered east from the prime meridian (0–360) and north from the equator (0–81), and vertical levels are numbered from the surface.

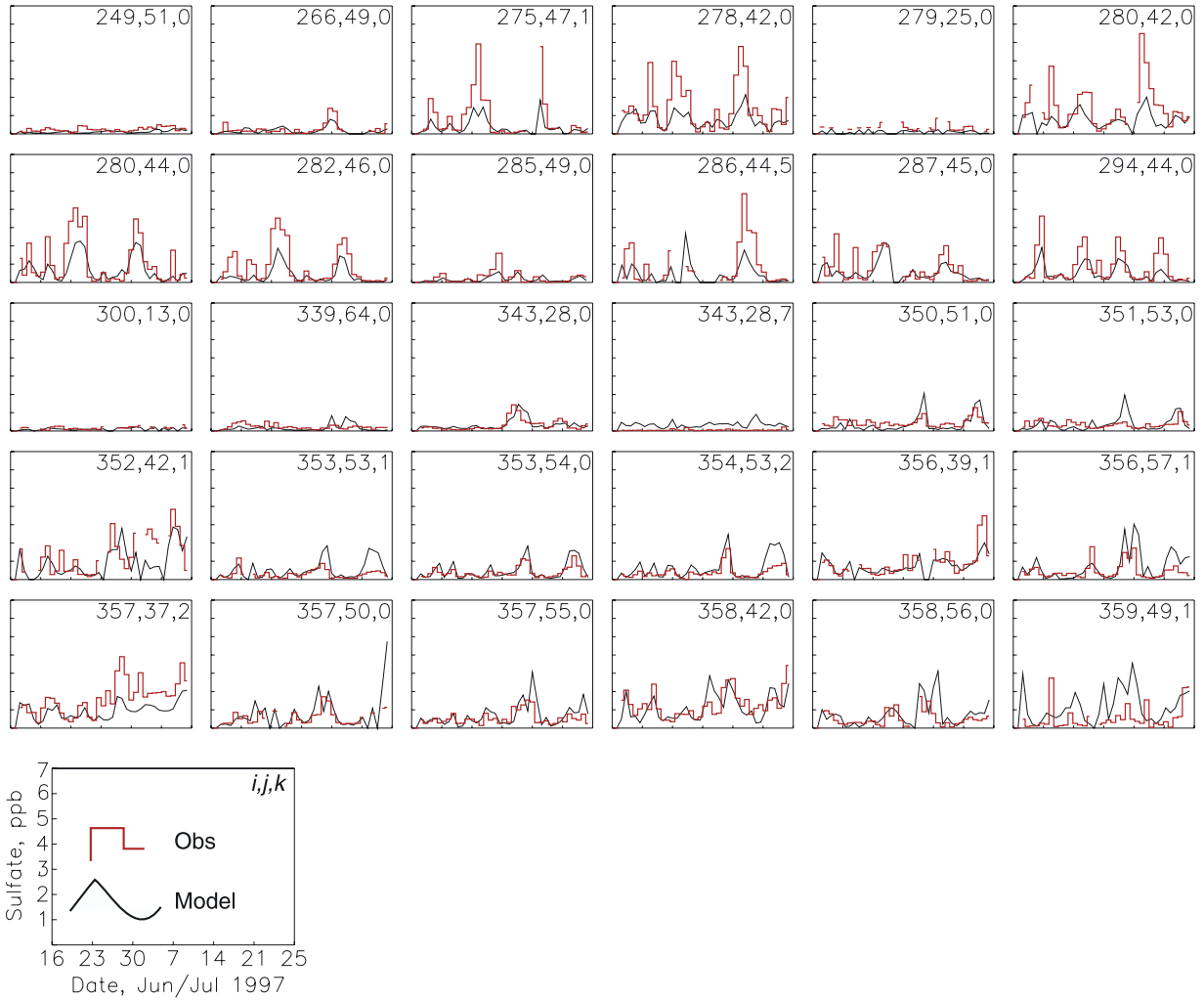


Figure 6. (continued)

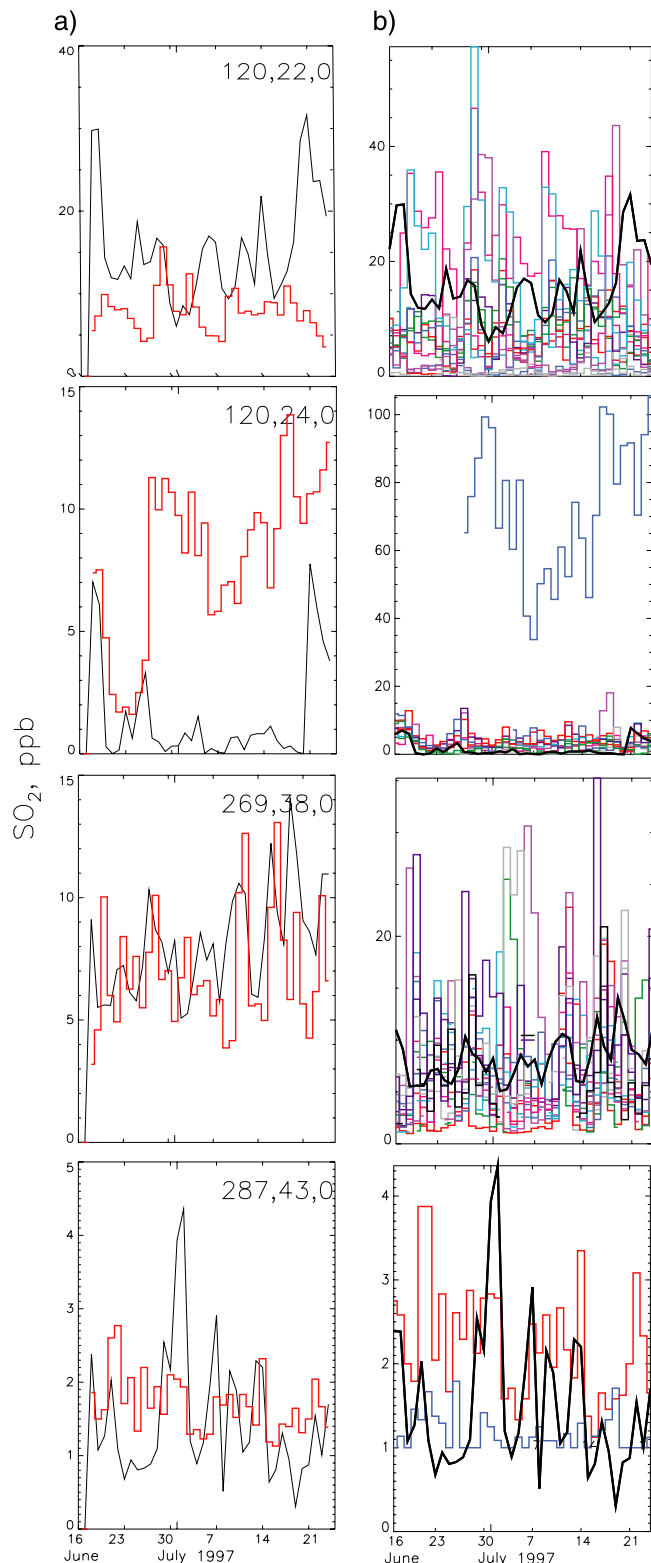


Figure 7. Examples of time series of SO₂ at locations with more than one station. Each horizontal pair of panels represents one model grid cell; the three numbers, x, y, z , at the top right of the left panel represent the three-dimensional model coordinates (i, j, k) of the location. In all panels the black lines represent the model results. In Figure 7a the cityscape red lines represent the average of all the observed mixing ratios. In Figure 7b the cityscape lines represent observed mixing ratios at individual stations within the model grid cell; the vertical spread of these lines on a given date represents the within-location spatial variability of the mixing ratios on that date. Note the artificial lower limit for reporting the observed mixing ratios for one station in the last panel.

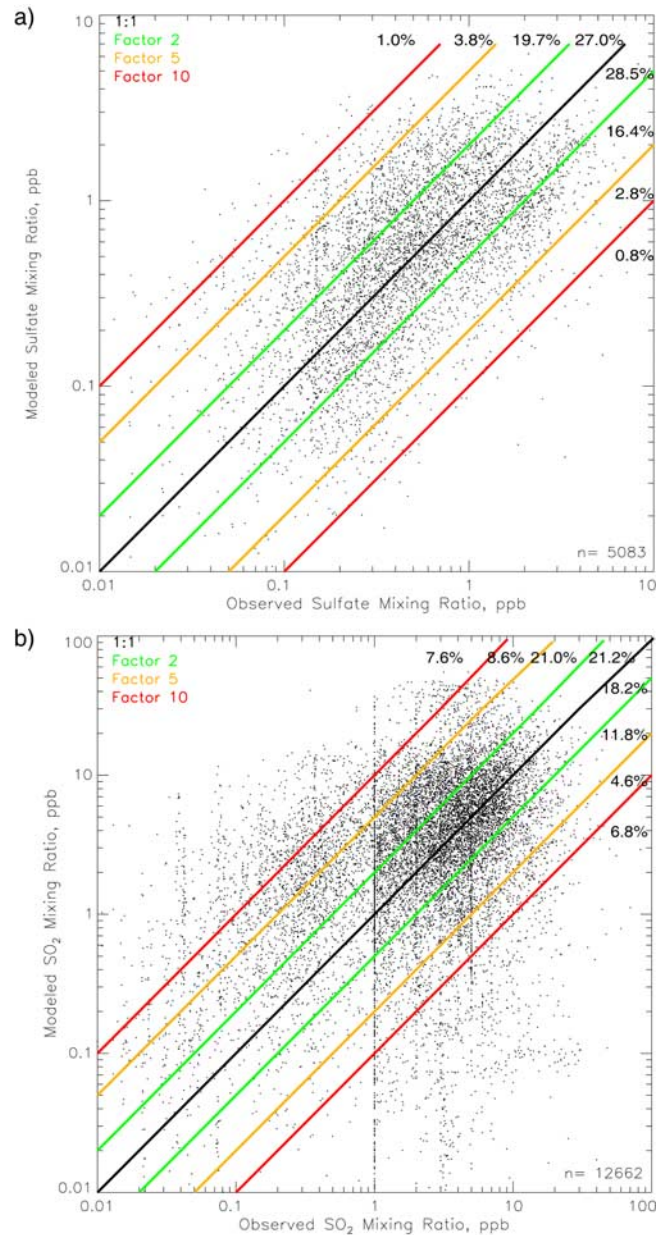


Figure 8. Scatterplots of modeled versus observed mixing ratios of (a) sulfate and (b) SO₂. Here, n indicates the number of cases in each plot. Observed SO₂ MRs in a straight line, especially evident at 1 ppb, were caused by an artificial setting of the lower limit of reporting for measurements; this is further illustrated in Figure 7.